An improved shear deformable theory for bending and buckling response of thin-walled FG sandwich I-beams resting on the elastic foundation

Ngoc-Duong Nguyen[a], Thuc P. Vo[b,*], Trung-Kien Nguyen[a,†]

[a] Faculty of Civil Engineering, Ho Chi Minh City University of Technology and Education, 1 Vo Van Ngan Street, Thu Duc District, Ho Chi Minh City, Viet Nam.

[b] School of Engineering and Mathematical Sciences, La Trobe University, Bundoora, VIC 3086, Australia

Abstract

This paper proposes an improved first-order beam theory by separation of variables for bending and buckling analysis of thin-walled functionally graded (FG) sandwich I-beams resting on a two-parameter elastic foundation. By dividing the displacements into bending and shear parts, this model can produce the deflections for both two cases with and without shear effect. The mechanical properties of beams based on the power law distribution of volume fraction of ceramic or metal. Governing equations are established from Lagrange's equations. The new Ritz's approximation functions, which are combined between orthogonal polynomial and exponential functions, are proposed to solve problem. The deflections and critical buckling loads of thin-walled FG sandwich I-beams are presented and compared with those available literature to verify the present theory. The effects of material distribution, boundary conditions, length-to-height ratio, shear deformation and foundation parameters on the results are investigated in detail.

Keywords: Ritz method; Bending behaviours; Buckling behaviours; FG sandwich I-beams

* Corresponding author.
E-mail address: t.vo@latrobe.edu.au
† Corresponding author.
E-mail address: kiennt@hcmute.edu.vn

1. Introduction

Functionally graded materials (FGM) are special types of composite materials, which are made from a mixture of metal and ceramic. They have advantages such as excellent corrosive resistance, high strength and stiffness-to-weight ratio, low thermal expansion, and especially, they meet stress continuity existing at surfaces of laminated composite. Therefore, FGM are increasingly used in many fields of mechanical, civil, marine, aerospace, defence, energy, electronic, medical, nuclear engineering [1]. Besides application in many engineering fields, a review study ([2]) indicates that FGM attracted huge researchers considered behaviours of FG structures. Many solution methods and models have been proposed for their accurate analysis, in which the static and buckling behaviours are the critical performance and interest of thin-walled FG beams.

Vlasov [3] firstly proposed the most straightforward thin-walled beam theory for isotropic material. Based on Vlasov's theory, there are many papers related to thin-walled composite beams and some are mentioned here [4-7] since this paper focuses on the thin-walled FG beams. Nguyen et al. [8], and Kim and Lee [9, 10] analysed bending behaviours of FG beams with the channel, I-section and box sections using Vlasov's theory. Blanc et al. [11] investigated nonlinear buckling responses of FG beams by finite element method. Librescu et al. [12] studied dynamic and buckling behaviours of simply-supported spinning thin-walled FG beams. Flexural-torsional and lateral buckling analysis of FG beams are also carried out in the studies ([13-15]). It can be seen that Vlasov's theory is just appropriate for slender beams because it neglects shear deformation effect. In order to account this effect, Kim and Lee [16] applied thin-walled composite beam model of Lee ([17]) to analyse flexural behaviours of FG I-beams. Kim

and Lee [18] investigated instability of FG I-beams considering shear deformation. Demirbas et al. [19] and Kvaternik et al. [20] proposed refined beam theory in the framework of the Carrera Unified Formulation (CUF) to evaluate bending response and nonlinear buckling response of FG beams. FG plates also attracted a large number of investigators. Khiloun et al. [21], Boussoula et al. [22] presented higher-order shear deformation theory for vibration and bending of FG plates. Vibration and buckling responses of FG nanoplates were also investigated by Balubaid et al. [23] and Karami et al. [24]. Hussain et al. [25] analysed fundamental natural frequency of FG cylindrical shell with ring supports. Thai and Choi [26, 27] presented simple first-order shear deformation theories by dividing the transverse displacement into bending and shear parts for vibration and bending analysis of composite and FG plates. In these studies, the proposed theories just contain four unknowns and have strong similarities. Generally, the idea of partitioning the displacement gives the displacement fields had simple forms, and reduces computational cost. Therefore, this approach is widely used in analysing behaviours of FG plates ([28-31]), and rectangular beams ([32-36]). However, it is interesting to state that it has not developed for the static and buckling response of thin-walled FG sandwich beams yet.

The behaviour of FG structures on elastic foundation is essential and interesting in engineering fields. A large number of models and idealization are proposed for the accurate response of structure on the foundation [37]. Li and Shao [38] analysed the nonlinear effect on bending behaviours of FG cantilever beams on Winkler foundation. Akbaş [39] presented deflections and frequencies of FG beams resting on Winkler foundation using classical and first-order beam theories. Gan and Nguyen [40] used two-parameter foundation model for nonlinear response of FG beams. Ying et al. [41]

proposed an exact elasticity solution for FG beams on elastic foundation. Esen [42] used two-parameter foundation model for dynamic response of FG Timoshenko beam. Fahsi et al. [43] studied structural responses of the FG beams on elastic foundation with the porosity effect. Chaabane et al. [44] investiagted bending and free vibration responses of FG beams resting on Winkler-Pasternak foundations. Matouk et al. [45] analysed hygro-thermal vibration of FG nanobeams on the elastic foundation using Hamilton principle and Navier method. Bousahla et al. [46] and Bourada et al. [47] presented buckling and vibration behaviours of SW-CNT-RC beams resting on foundation with simply supported boundary condition based on first shear deformation theory. Besides papers dealing with responses of FG beams ([38-47]), there are many studies investigated behaviours of FG plates on elastic foundation. Rabhi et al. [48], Chikr et al. [49], Kaddari et al. [50], and Rahmani et al. [51] proposed models for buckling, bending and vibrations analysis of FG plates resting on elastic foundations. Effects of two-parameter elastic foundation on hygro-thermo-mechanical buckling and bending analysis of FG plates are investigated by Refrafi et al. [52] and Tounsi et al. [53]. Shariati et al. [54] and Furjan et al. [55] studied vibration and stability of multi-scale hybrid disk based on nonlinear elastic foundation. Although there are many papers investigated effects of elastic foundation on responses of FG beams and plates as far as the authors are aware there is no study that considers both shear and foundation effects for bending and buckling behaviours of thin-walled FG I-beams.

For the computational method, although the finite element method is used popularly for analysis of thin-walled FG beams [11, 13-15, 56, 57], many investigators proposed Ritz method for FG beams with rectangular section [58-62]. Nguyen et al. [63] developed Ritz functions for buckling and vibration behaviours of FG and laminated

composite thin-walled beams. It can be stated that Ritz method is rarely used for analysis of the thin-walled FG beams.

The main contributions of this paper are to propose 1) an improved first-order beam theory for thin-walled FG I-beams using separation of variables and 2) new Ritz-functions for their deflections and buckling loads resting on elastic foundation. This model can produce the results for both with and without shear effect due to dividing the displacements into bending and shear parts. The displacements and buckling loads are presented and compared with those available literature to verify the present theory. The effects of ceramic thickness ratio, material parameter, length-to-height ratio, boundary conditions, shear deformation and foundation parameters on the results are examined. Some of the new results is presented for the first time as a benchmark for reference in the future.

2. Theoretical formulation

Consider a thin-walled FG beam as indicated in Fig. 1. There are three coordinate systems required to develop the displacement field of the beam as follows: the Cartesian coordinate system (y, z, x), local plate coordinate system (n, s, x), and contour coordinate s which draws along the profile of the section. φ_s is an angle of orientation between (y, z, x) and (n, s, x) coordinate systems. $P\left(y_P, \mathrm{z}_P\right)$ is shear center of cross-section [6]. To establish displacement field of thin-walled FG beam, the following assumptions are accepted:

1) The contour of thin-walled cross-section does not deform in its own plane.
2) Shear strains $\gamma_{yx}^0, \gamma_{zx}^0$ and warping shear γ_{ϖ}^0 are uniform over the section.
3) Poisson ratio is constant.

2.1. Kinematics

The mid-surface displacement ($\bar{v},\bar{w}$) at a point in contour are given in terms of the rotation angle ϕ about the pole axis and displacements *V, W* of the pole *P* in the *y, z*-directions, respectively as follows:

$$\bar{v}(s,x)=V(x)\sin\varphi_s(s)-W(x)\cos\varphi_s(s)-\phi(x)q(s) \tag{1a}$$

$$\bar{w}(s,x)=V(x)\cos\varphi_s(s)+W(x)\sin\varphi_s(s)+\phi(x)r(s) \tag{1b}$$

By using separation of variables [26-28], it is convenient to divide the displacements into bending part, denoted by the subscript *b* and shear part, denoted by the subscript *s* as follows:

$$V(x)=V_b(x)+V_s(x) \tag{2a}$$

$$W(x)=W_b(x)+W_s(x) \tag{2b}$$

$$\phi(x)=\phi_b(x)+\phi_s(x) \tag{2c}$$

The out-of-plane plate displacement $\bar{u}$ is determined according to the assumption (2). The shear strains at mid-surface of the plate can be defined as follows:

$$\bar{\gamma}_{nx}(s,x)=V_s'(x)\sin\varphi_s(s)-W_s'(x)\cos\varphi_s(s)-\phi_s'(x)q(s) \tag{3a}$$

$$\bar{\gamma}_{sx}(s,x)=V_s'(x)\cos\varphi_s(s)+W_s'(x)\sin\varphi_s(s)+\phi_s'(x)r(s) \tag{3b}$$

where the prime superscript indicates differentiation with respect to *x*. From the definition of the shear strain, $\bar{\gamma}_{sx}$ at mid-surface of each element can be expressed as [16]:

$$\bar{\gamma}_{sx}(s,x)=\frac{\partial\bar{w}}{\partial x}+\frac{\partial\bar{u}}{\partial s} \tag{4}$$

By substituting $\bar{w}$ from Eq. (1b) into Eq. (4) and using Eq. (2), displacement $\bar{u}$ can be written by:

$$\bar{u}(s,x)=U(x)-V_b'(x)y(s)-W_b'(x)z(s)-\phi_b'(x)\varpi(s) \tag{5}$$

where ϖ is the warping function:

$$\varpi(s)=\int_{s_0}^{s} r(s)ds \tag{6}$$

The displacement components (*v, w, u*) at an arbitrary point on the cross-section are given with respect to the mid-surface displacements ($\bar{v}$, $\bar{w}$, $\bar{u}$) as follows:

$$v(n,s,x)=\bar{v}(s,x) \tag{7a}$$

$$w(n,s,x)=\bar{w}(s,x)+n\bar{\psi}_s(s,x) \tag{7b}$$

$$u(n,s,x)=\bar{u}(s,x)+n\bar{\psi}_x(s,x) \tag{7c}$$

where $\bar{\psi}_x$ and $\bar{\psi}_s$ are the rotations of transverse normal about *x* and *s*, respectively. $\bar{\psi}_x$ can be expressed by definition of the mid-surface shear strains γ_{nx} as below:

$$\bar{\gamma}_{nx}(s,x)=\frac{\partial\bar{u}}{\partial n}+\frac{\partial\bar{v}}{\partial x}=\bar{\psi}_x(s,x)+\frac{\partial\bar{v}}{\partial x} \tag{8}$$

By comparing Eq.(3) and (8), the function $\bar{\psi}_x(s,x)$ can be obtained as:

$$\bar{\psi}_x(s,x)=-V_b^{'}(z)\sin\varphi_s(s)+W_b^{'}(x)\cos\varphi_s(s)+\phi_b^{'}(x)q(s) \tag{9}$$

Similarly, $\bar{\psi}_s$ can be written by using the assumption that the shear strain γ_{sn} should vanish at mid-surface of each element:

$$\bar{\psi}_s(s,x)=-\frac{\partial v}{\partial s}=\phi_b(x)+\phi_s(x) \tag{10}$$

The non-zero strains of thin-walled FG beam are expressed by:

$$\begin{aligned}\varepsilon_x(n,s,x)&=\bar{\varepsilon}_x(s,x)+n\bar{\kappa}_x(s,x)=\varepsilon_x^0+(y+n\sin\varphi_s)\kappa_z+(z-n\cos\varphi_s)\kappa_y+(\varpi-nq)\kappa_{\varpi}\\&=U^{'}-(y+n\sin\varphi_s)V_b^{''}-(z-n\cos\varphi_s)W_b^{''}-(\varpi-nq)\phi_b^{''}\end{aligned} \tag{11a}$$

$$\begin{aligned}\gamma_{sx}(n,s,x)&=\bar{\gamma}_{sx}(s,x)+n\bar{\kappa}_{sx}(s,x)=\gamma_{yx}^0\cos\varphi_s+\gamma_{zx}^0\sin\varphi_s+\gamma_{\varpi}^0 r+n\kappa_{sx}\\&=V_s^{'}\cos\varphi_s+W_s^{'}\sin\varphi_s+\phi_s^{'}r+(2\phi_b^{'}+\phi_s^{'})n\end{aligned} \tag{11b}$$

$$\begin{aligned}\gamma_{nx}(n,s,x)&=\bar{\gamma}_{nx}(s,x)+n\bar{\kappa}_{nx}(s,x)=\gamma_{yx}^{0}\sin\varphi_s-\gamma_{zx}^{0}\cos\varphi_s-\gamma_{\varpi}^{0}q\\&=V_s^{'}\sin\varphi_s-W_s^{'}\cos\varphi_s-\phi_s^{'}q\end{aligned}\tag{11c}$$

where

$$\varepsilon_x^0=U^{'}\tag{12a}$$

$$\gamma_{yx}^0=V_s^{'}\tag{12b}$$

$$\gamma_{zx}^0=W_s^{'}\tag{12c}$$

$$\gamma_{\varpi}^0=\phi_s^{'}\tag{12d}$$

$$\kappa_y=-W_b^{''}\tag{12e}$$

$$\kappa_z=-V_b^{''}\tag{12f}$$

$$\kappa_{\varpi}=-\phi_b^{''}\tag{12g}$$

$$\kappa_{sx}=2\phi_b^{'}+\phi_s^{'}\tag{12h}$$

2.2. Constitutive relations

Young's modulus of thin-walled section is defined via Young's modulus of metal (E_m) and ceramic (E_c) as well as volume fraction of ceramic (V_c):

$$E=E_cV_c+E_m(1-V_c)\tag{13}$$

Two types of the material distributions are considered as follows (Fig. 2):

Type A: for the top and bottom flanges

$$V_c=\left[\frac{n+0.5h}{(1-\alpha)h}\right]^p,\quad -0.5h\le n\le(0.5-\alpha)h\tag{14a}$$

$$V_c=1,\quad (0.5-\alpha)h\le n\le 0.5h\tag{14b}$$

where p, $\alpha\,(\alpha_1,\alpha_2)$ and $h\,(h_1,h_2)$ are material parameter, ceramic thickness ratio and thickness of the top and bottom flanges, respectively.

Type B: for the web, top and bottom flanges

$$V_c = \left[\frac{-|n| + 0.5h}{0.5(1-\alpha)h}\right]^p, \quad -0.5h \le n \le -0.5\alpha h \quad \text{or} \quad 0.5\alpha h \le n \le 0.5h \tag{15a}$$

$$V_c = 1, \quad -0.5\alpha h \le n \le 0.5\alpha h \tag{15b}$$

where $\alpha\ (\alpha_1, \alpha_2, \alpha_3)$ and $h\ (h_1, h_2, h_3)$ are ceramic thickness ratio and thickness of the flange and web, respectively.

The stress and strain relations are defined as follows:

$$\begin{Bmatrix} \sigma_x \\ \sigma_{sx} \\ \sigma_{nx} \end{Bmatrix} = \begin{pmatrix} Q_{11}^* & 0 & 0 \\ 0 & Q_{66}^* & 0 \\ 0 & 0 & Q_{55}^* \end{pmatrix} \begin{Bmatrix} \varepsilon_x \\ \gamma_{sx} \\ \gamma_{nx} \end{Bmatrix} \tag{16}$$

where $$Q_{11}^* = E(n), \quad Q_{66}^* = Q_{55}^* = \frac{E(n)}{2(1+\nu)} \tag{17}$$

where ν is Poisson's ratio

2.3. Variational formulation

The strain energy Π_E of the system is defined through volume Ω by:

$$\Pi_E = \frac{1}{2}\int_\Omega \left(\sigma_x \varepsilon_x + \sigma_{sx}\gamma_{sx} + \sigma_{nx}\gamma_{nx}\right) d\Omega \tag{18}$$

Substituting Eqs. (11) and (16) into Eq. (18) leads to:

$$\Pi_E = \frac{1}{2}\int_0^L \begin{bmatrix} E_{11}U^{'2} - 2E_{12}U^{'}V_b^{''} - 2E_{13}U^{'}W_b^{''} - 2\left(E_{14}U^{'}\phi_b^{''} - 2E_{15}U^{'}\phi_b^{'}\right) \\ +2E_{16}U^{'}V_s^{'} + 2E_{17}U^{'}W_s^{'} + 2\left(E_{15}+E_{18}\right)U^{'}\phi_s^{'} + E_{22}V_b^{''2} + 2E_{23}V_b^{''}W_b^{''} + 2E_{24}V_b^{''}\phi_b^{''} \\ -4E_{25}V_b^{''}\phi_b^{'} - 2E_{26}V_b^{''}V_s^{'} - 2E_{27}V_b^{''}W_s^{'} - 2\left(E_{25}+E_{28}\right)V_b^{''}\phi_s^{'} + E_{33}W_b^{''2} \\ +2E_{34}W_b^{''}\phi_b^{''} - 4E_{35}W_b^{''}\phi_b^{'} - 2E_{36}W_b^{''}V_s^{'} - 2E_{37}W_b^{''}W_s^{'} - 2\left(E_{35}+E_{38}\right)W_b^{''}\phi_s^{'} + E_{44}\phi_b^{''2} \\ -4E_{45}\phi_b^{''}\phi_b^{'} + 4E_{55}\phi_b^{'2} - 2E_{46}\phi_b^{''}V_s^{'} + 4E_{56}\phi_b^{'}V_s^{'} - 2E_{47}\phi_b^{''}W_s^{'} + 4E_{57}\phi_b^{'}W_s^{'} \\ -2\left(E_{45}+E_{48}\right)\phi_b^{''}\phi_s^{'} + 4\left(E_{55}+E_{88}\right)\phi_b^{'}\phi_s^{'} + E_{66}V_s^{'2} + 2E_{67}V_s^{'}W_s^{'} + 2\left(E_{56}+E_{68}\right)V_s^{'}\phi_s^{'} \\ +E_{77}W_s^{'2} + 2\left(E_{57}+E_{78}\right)W_s^{'}\phi_s^{'} + \left(E_{55}+2E_{58}+E_{88}\right)\phi_s^{'2} \end{bmatrix} dx \tag{19}$$

where: E_{ij} are the stiffness of thin-walled FG I-beams, which are defined in **Appendix**

A; L is the length.

The elastic foundation energy Π_F of the system is defined by [64, 65]:

$$\Pi_F = \frac{1}{2}\int_0^L \begin{bmatrix} k_y\left\{V_b + V_s - \left(\phi_b + \phi_s\right)\left(l_y - y_p\right)\right\}^2 + k_z\left\{W_b + W_s + \left(\phi_b + \phi_s\right)\left(l_z - z_p\right)\right\}^2 \\ +k_t\left(\phi_b + \phi_s\right)^2 + g_y\left\{V_b^{'} + V_s^{'} - \left(\phi_b^{'} + \phi_s^{'}\right)\left(l_y - y_p\right)\right\}^2 \\ +g_z\left\{W_b^{'} + W_s^{'} + \left(\phi_b^{'} + \phi_s^{'}\right)\left(l_z - z_p\right)\right\}^2 \end{bmatrix} dx \quad (20)$$

where k_y and g_y as well as k_z and g_z are the first and second foundation parameters in *y*- and *z*-direction respectively; k_t is the rotational parameter for rotation of the cross-section; and $\left(l_y, l_z\right)$ are the coordinate of transverse translation point as shown in Fig. 3.

The potential energy Π_W by external forces, which are axial load N_0, uniformed transverse load q_z and concentrated transverse load P_z applied at x_L, can be expressed as [17, 63]:

$$\begin{aligned} \Pi_W = &\int_0^L N_0 \begin{Bmatrix} \left(V_b^{'} + V_s^{'}\right)^2 + \left(W_b^{'} + W_s^{'}\right)^2 + 2z_P\left(V_b^{'} + V_s^{'}\right)\left(\phi_b^{'} + \phi_s^{'}\right) \\ -2y_P\left(W_b^{'} + W_s^{'}\right)\left(\phi_b^{'} + \phi_s^{'}\right) + \dfrac{I_P}{A}\left(\phi_b^{'} + \phi_s^{'}\right)^2 \end{Bmatrix} dx \\ &+ \int_0^L q_z\left(W_b + W_s\right) dx + P_z\left(W_b + W_s\right) x_L \end{aligned} \quad (21)$$

2.4. Ritz solution

By using Ritz's approximation functions which combined between orthogonal polynomial and exponential functions, the displacement fields can be written as:

$$U(x) = \sum_{j=1}^{m} \zeta_j^{'}(x) U_j \quad (22a)$$

$$V_b(x) = \sum_{j=1}^{m} \zeta_j(x) V_{bj} \quad (22b)$$

$$W_b(x) = \sum_{j=1}^{m} \zeta_j(x) W_{bj} \tag{22c}$$

$$\phi_b(x) = \sum_{j=1}^{m} \zeta_j(x) \phi_{bj} \tag{22d}$$

$$V_s(x) = \sum_{j=1}^{m} \zeta_j(x) V_{sj} \tag{22b}$$

$$W_s(x) = \sum_{j=1}^{m} \zeta_j(x) W_{sj} \tag{22c}$$

$$\phi_s(x) = \sum_{j=1}^{m} \zeta_j(x) \phi_{sj} \tag{22d}$$

where U_j, V_{bj}, W_{bj}, ϕ_{bj}, V_{sj}, W_{sj} and ϕ_{sj} are Ritz's parameter and $\zeta_j(x)$ are Ritz's approximation functions, which satisfy with various boundary conditions (BCs) as indicated in Table 1.

The deflections and buckling loads of the beams can be obtained by using total potential energy (Π) and Lagrange's equations:

$$\Pi = \Pi_E + \Pi_F - \Pi_W \tag{23}$$

$$\frac{\partial \Pi}{\partial p_j} = 0 \tag{24}$$

where p_j representing the values of U_j, V_{bj}, W_{bj}, ϕ_{bj}, V_{sj}, W_{sj} and ϕ_{sj}

$$\begin{bmatrix} \mathbf{K}^{11} & \mathbf{K}^{12} & \mathbf{K}^{13} & \mathbf{K}^{14} & \mathbf{K}^{15} & \mathbf{K}^{16} & \mathbf{K}^{17} \\ {}^{T}\mathbf{K}^{12} & \mathbf{K}^{22} & \mathbf{K}^{23} & \mathbf{K}^{24} & \mathbf{K}^{25} & \mathbf{K}^{26} & \mathbf{K}^{27} \\ {}^{T}\mathbf{K}^{13} & {}^{T}\mathbf{K}^{23} & \mathbf{K}^{33} & \mathbf{K}^{34} & \mathbf{K}^{35} & \mathbf{K}^{36} & \mathbf{K}^{37} \\ {}^{T}\mathbf{K}^{14} & {}^{T}\mathbf{K}^{24} & {}^{T}\mathbf{K}^{34} & \mathbf{K}^{44} & \mathbf{K}^{45} & \mathbf{K}^{46} & \mathbf{K}^{47} \\ {}^{T}\mathbf{K}^{15} & {}^{T}\mathbf{K}^{25} & {}^{T}\mathbf{K}^{35} & {}^{T}\mathbf{K}^{45} & \mathbf{K}^{55} & \mathbf{K}^{56} & \mathbf{K}^{57} \\ {}^{T}\mathbf{K}^{16} & {}^{T}\mathbf{K}^{26} & {}^{T}\mathbf{K}^{36} & {}^{T}\mathbf{K}^{46} & {}^{T}\mathbf{K}^{56} & \mathbf{K}^{66} & \mathbf{K}^{67} \\ {}^{T}\mathbf{K}^{17} & {}^{T}\mathbf{K}^{27} & {}^{T}\mathbf{K}^{37} & {}^{T}\mathbf{K}^{47} & {}^{T}\mathbf{K}^{57} & {}^{T}\mathbf{K}^{67} & \mathbf{K}^{77} \end{bmatrix} \begin{Bmatrix} \mathbf{U} \\ \mathbf{V_b} \\ \mathbf{W_b} \\ \mathbf{\Phi_b} \\ \mathbf{V_s} \\ \mathbf{W_s} \\ \mathbf{\Phi_s} \end{Bmatrix} = \begin{Bmatrix} \mathbf{0} \\ \mathbf{0} \\ \mathbf{F_b} \\ \mathbf{0} \\ \mathbf{0} \\ \mathbf{F_s} \\ \mathbf{0} \end{Bmatrix} \tag{25}$$

where the stiffness matrix **K** and vetor **F** are expressed in **Appendix B**.

3. Numerical results

The numerical examples are carried out to analyse bending and buckling responses of thin-walled FG I-beams, and verify the proposed theory. S1-section with Type A for flanges and Type B for web (Fig.2a), and S2-section with Type B for both flanges and web (Fig.2b) are considered. These configurations meet continuity of FG at flanges and web connection. This makes the relation between web and flanges becomes stronger, and the approach presented is feasible [8, 11, 16]. Material properties are given by $E_m = 105.69\text{x}10^6\, kN/m^2$, $E_c = 320.7\text{x}10^6\, kN/m^2$ and $\nu_m = \nu_c = 0.3$. Ratio $W_s/W\,\text{x}100\%$ is defined as the shear effect. The effects of material distribution, material parameter (p), BCs, length-to-height ratio (L/b_3), shear deformation, and foundation parameters on the results are examined.

3.1. Convergence study

To study the convergence of present solution, the FG I-beams ($h_1 = h_2 = h_3 = h = 0.005m$, $b_1 = b_2 = 0.1m$, $b_3 = 0.2m$, $L = 2.5m$, $\alpha_1 = \alpha_2 = 0.7$, $\alpha_3 = 0.4$, $p = 5$, S1-section) are considered. For static problem, the concentrated transverse load $(P_z = 100\,kN)$ acts at mid-span of beams. The buckling loads and mid-span deflections of various beams are shown in Table 2. It can be found that the present solution converges at m = 10 for deflection and m = 8 for buckling. Therefore, these numbers are selected for the following examples.

3.2. Bending analysis

3.2.1. Verification

In order to verify the beam model and solution, the simply-supported isotropic I-beam ($h_1 = h_2 = h_3 = h = 0.00208m$, $b_1 = b_2 = b_3 = 0.05m$, $L = 2.5m$) is considered.

The Poisson ratio and Young's modulus are assumed to be $\nu = 0.25$ and $E = 53.78\text{x}10^6\, kN/m^2$. The maximum deflections of beams subjected to the concentrated transverse load ($P_z = 1kN$) at mid-span are compared with those of Kim and Lee [16] in Table 3. The present results have coincided with previous results [16] for both cases with and without shear effect.

A cantilever FG I-beam ($h_1 = h_2 = h_3 = h = 0.002m$, $b_1 = 20h$, $b_2 = 10h$, $b_3 = 40h$, $L = 2.5m$, $\alpha_1 = 0.9$, $\alpha_2 = 0.1$, $\alpha_3 = 0.4$, S1-section) subjected to a concentrated transverse load (P_z) acting at the free end is examined. For comparison with the available literature, the nondimensional deflection is defined by $\bar{W} = \dfrac{E_c h b_3^3}{P_z L^3}$. The maximum deflections again agree well with previous results [16] in Table 4. Since there is no published data for the FG I-beams resting on elastic foundation, a cantilever composite I-beam ($h_1 = 0.00208m$, $h_2 = 0.00312m$, $h_3 = 0.00104m$, $b_1 = 0.03m$, $b_2 = 0.04m$, $b_3 = 0.05m$, $L = 2.5m$) is considered. Material properties are as follows: $E_1 = 53.78\text{x}10^6\, kN/m^2$, $E_2 = E_3 = 17.93\text{x}10^6\, kN/m^2$, $G_{12} = G_{13} = 8.96\text{x}10^6\, kN/m^2$, $G_{23} = 3.45\text{x}10^6\, kN/m^2$, $\nu_{12} = \nu_{13} = 0.25$ and $\nu_{23} = 0.34$. Lay-ups are $[30/-30]_{4S}$ for top flange, $[30/-30]_{6S}$ for bottom flange, and $[30/-30]_{2S}$ for web. Table 5 displays the maximum deflections of beams subjected to a concentrated transverse load $(P_z = 0.1kN)$ acting at the free end respect to foundation parameters k_z and g_z. It is seen that the present results are again in excellent agreement with those of Kim and Lee [4].

3.2.2 Thin-walled FG I-beams without foundation effect

The effects of p, L/b_3, BCs, and material distribution on the deflections of beams are investigated. The FG I-beams ($h_1=h_2=h_3=h=0.002m$, $b_1=20h$, $b_2=10h$, $b_3=40h$) are considered. Tables 6 and 7 show their mid-span deflections ($L/b_3=10$ and $L/b_3=20$) subjected to the concentrated transverse load ($P_z=10kN$) acting at mid-span for S1-section ($\alpha_1=0.9, \alpha_2=0.1, \alpha_3=0.4$) and S2-section ($\alpha_1=0.1, \alpha_2=0.1, \alpha_3=0.1$), respectively. It is clear that beams' deflections increase as L/b_3 and p increase for both S1- and S2-sections. This is reasonable because the portion of ceramic volume fraction directly depends on p and it leads to a reduction in stiffness when *p* increases [13]. It is seen from Tables 6 and 7 that the deflections are the largest for C-F beams and the smallest for C-C ones as predicted. Fig. 4 displays the variation of shear effect respect to the L/b_3 for S1- and S2-section, respectively. The shear effect decreases as the L/b_3 increases as expected, and it is the largest for C-C beams.

To investigate the effect of ceramic thickness ratio on the shear effect, FG C-C I-beams ($h_1=h_2=h_3=h=0.002m$, $b_1=20h$, $b_2=10h$, $b_3=40h$, $L=8b_3$, S1-section) under a uniformly distributed transverse load ($q_z=0.5kN/m$) are considered. Figs. 5a-7a show variation of the shear effect respect to ceramic thickness ratio in flanges and web. The ceramic thickness ratio affects significantly to the shear effect, and 1) the shear effect decreases as the ceramic thickness ratio in web increases; 2) as the ceramic thickness ratio of top flange increases, the shear effect increases and then decreases; and 3) the shear effect increases as the ceramic thickness ratio in bottom flange increases. These phenomenons can be explained in Figs. 5b-7b which display the variation of ratios of flexural and shear rigidity (E_{33}/E_{77}) respect to ceramic thickness ratio. It can be concluded that variation of the shear effect depends on the (E_{33}/E_{77}) ratio which are defined by material properties, material distribution and profile of cross-

section.

3.2.3. Thin-walled FG I-beams with foundation effect

The FG I-beams ($h_1 = h_2 = h_3 = h = 0.002m$, $b_1 = 20h$, $b_2 = 10h$, $b_3 = 40h$, $p = 10$, $L = 20b_3$, $q_z = 5kN/m$) resting on two-parameter foundation in the *z*-direction are considered as shown in Fig. 8. Tables 8 and 9 show their mid-span deflections respect to foundation parameters for S1-section $(\alpha_1 = 0.9, \alpha_2 = 0.1, \alpha_3 = 0.4)$ and S2-section $(\alpha_1 = \alpha_2 = \alpha_3 = 0.1)$, respectively. It is seen that the deflections decrease as foundation parameters increase for both S1- and S2-section because the increase of foundation parameters makes beams get stiffer.

To further investigate the effect of foundation parameters, the FG I-beams ($h_1 = h_2 = h_3 = h = 0.002m$, $b_1 = 20h$, $b_2 = 10h$, $b_3 = 40h$, $p = 10$, $L = 20b_3$, $\alpha_1 = 0.9, \alpha_2 = 0.1, \alpha_3 = 0.4$, S1-section) with four cases are considered as follows: Case 1 ignores the foundation effect; Case 2 considers the first parameter of foundation; Case 3 considers the second parameter of foundation, and both two parameters of the foundation are considered in Case 4. Soil sub-grade properties are assumed to be $g_z = 282.150kN$ and $K_s = 1007kN/m^3$ [4]. For beam with bottom width $b_2 = 10h = 0.02m$, the first foundation parameter is determined $k_z = K_s b_2 = 20.140kN/m^2$. Fig. 9a and b display the deflections of the C-C and C-S beams under uniformly distributed transverse load ($q_z = 20kN/m$), respectively. It is seen from these figures that the first foundation parameter does not have strong effect to beams' deflections. However, the second one causes the decrease of maximum deflections about 25% and 38% for C-C and C-S beam, respectively.

Figs. 10 and 11 display the ratio of deflection between the first and second

foundation parameters for various BCs. It can be seen from Fig. 10 that in case of small L/b_3 ratio ($L/b_3 \le 20$), the effect of the first foundation parameter is negligible, but it becomes very significant as L/b_3 ratio is large $(L/b_3 = 70)$. Fig. 11 indicates that the effect of second foundation parameters is noticeable, and increases as L/b_3 increases. It is the smallest for C-C beams and the largest for C-F ones. It can be concluded from present results that the effect of foundation parameters becomes very remarkable as stiffness of beams reduces.

3.3. Buckling analysis

3.3.1. Thin-walled FG I-beams without foundation effect

For verification purpose, FG I-beams ($h_1 = h_2 = h_3 = h = 0.005m$, $b_1 = b_2 = 0.1m$, $b_3 = 0.2m$, $L = 2.5m$) with $\alpha_1 = \alpha_2 = \alpha_3 = 0.4$, S2-section and $\alpha_1 = \alpha_2 = 0.7$, $\alpha_3 = 0.4$, S1-section are considered. Their critical buckling loads (kN) with various BCs are printed in Tables 10-14, and are compared with those with and without shear effect ([11, 18, 63]). It shows an excellent agreement of present results with those from previous results. Figs. 12 and 13 show the effect of ceramic thickness ratio in flanges (as $\alpha_3 = 0.4$) and web (as $\alpha_1 = \alpha_2 = 0.7$) on the first three buckling loads of C-S beams ($p = 10$). It can be seen from these figures that the results increase significantly as the ceramic thickness ratio in flanges increases, however, they just slightly increase as the ceramic thickness ratio in web increases. This is due to the fact that the increase of ceramic thickness ratio in flanges causes noticeable increase of the bending and torsional rigidities of beams.

The FG I-beams ($h_1 = h_2 = h_3 = h = 0.005m$, $b_1 = b_2 = 0.1m$, $b_3 = 0.05m$, $p = 10$, $\alpha_1 = \alpha_2 = \alpha_3 = 0.4$, S2-section) with $L/b_3 = 10$ and $L/b_3 = 50$ are considered to

investigate shear effect. Figs. 14-17 show the first four buckling mode shapes of beams for $L/b_3 = 10$ and $L/b_3 = 50$. From these figures, it is clear that the contribution of shear mode is significant for lower length-to-height ratio ($L/b_3 = 10$) and higher buckling mode (Modes 2 and 4).

3.3.3. Thin-walled FG I-beams with foundation effect

To evaluate foundation effect on the critical buckling loads, S1-section ($\alpha_1 = \alpha_2 = 0.7, \alpha_3 = 0.4$) and S2-section ($\alpha_1 = \alpha_2 = \alpha_3 = 0.4$) with geometry ($h_1 = h_2 = h_3 = h = 0.005m$, $b_1 = b_2 = 0.1m$, $b_3 = 0.05m$, $p = 10$, $L/b_3 = 50$) are considered. Figs. 18 and 19 display the variation of first four buckling loads of cantilever beams for S1- and S2-section respect to k_z and g_z. It is seen that the buckling modes in *z*-direction increase almost linearly as foundation parameter increases, and the buckling modes in *y*-direction do not affect by variation of foundation parameters because k_z and g_z just cause increase of beams's rigidity in *z*-direction.

Finally, the effects of BCs, L/b_3 on the critical buckling loads are investigated. The thin-walled FG beams with sections as in previous example are considered. Soil properties are assumed to be $g_z = 282.150kN$ and $k_z = 100.7kN/m^2$. Ratio $r_f = P_{1f}/P_1$ is defined to investigate the effect of BCs and L/b_3, where P_{1f} and P_1 are the critical buckling loads of beams with and without foundation effect, respectively. Fig. 20a and b show the variation of r_f respect to L/b_3 for various BCs for S1- and S2-sections. It is seen from these figures that r_f ratio increases as L/b_3 ratio increases until the critical buckling load of beams with foundation effect equals to the second buckling load of beams without it. It is mean now that r_f equals to ratio of the

second buckling load and critical buckling load of beams without foundation effect, and it is interesting that this ratio does not depend on boundary conditions.

4. Conclusions

An improved first-order beam theory, which is based on dividing the displacements into bending and shear part, is proposed for the static and buckling response of thin-walled FG I-beams. The presented beam model has straightforward form, and it is convenient to establish formula and solve the problems. In addition, this model can produce the results for both two cases with and without shear effect, therefore, it reduces computational cost in case of comparing shear effect. The effects of material distributions, length-to-height ratio, boundary conditions and foundation parameters on the displacement and critical buckling load of thin-walled FG I-beams are considered. Foundation parameters significantly affect to the deflections and critical buckling loads of beams. The proposed beam model is efficient for considering the shear effect on the static and buckling responses of thin-walled FG I-beams.

Appendix A: The stiffness E_{ij} of thin-walled FG beam are given:

$$E_{11}=\iint_A Q_{11}^* dnds,\quad E_{12}=\iint_A Q_{11}^*\left(y+n\sin\varphi_s\right)dnds,\quad E_{13}=\iint_A Q_{11}^*\left(z-n\cos\varphi_s\right)dnds$$

$$E_{14}=\iint_A Q_{11}^*\left(\varpi-nq\right)dnds,\quad E_{15}=E_{16}=E_{17}=E_{18}=0$$

$$E_{22}=\iint_A Q_{11}^*\left(y^2+2ny\sin\varphi_s+n^2\sin^2\varphi_s\right)dnds$$

$$E_{23}=\iint_A Q_{11}^*\left\{yz+n\left(z\sin\varphi_s-y\cos\varphi_s\right)-n^2\sin\varphi_s\cos\varphi_s\right\}dnds$$

$$E_{24}=\iint_A Q_{11}^*\left\{y\varpi+n\left(\varpi\sin\varphi_s-qy\right)-qn^2\sin\varphi_s\right\}dnds,\quad E_{25}=E_{26}=E_{27}=E_{28}=0$$

$$E_{33}=\iint_A Q_{11}^*\left(z^2-2nz\cos\varphi_s+n^2\cos^2\varphi_s\right)dnds$$

$$E_{34}=\iint_A Q_{11}^*\left\{z\varpi-n\left(\varpi\cos\varphi_s+qz\right)+qn^2\cos\varphi_s\right\}dnds,\quad E_{35}=E_{36}=E_{37}=E_{38}=0$$

$$E_{44}=\iint_A Q_{11}^*\left(\varpi^2-2n\varpi q+n^2q^2\right)dnds,\quad E_{45}=E_{46}=E_{47}=E_{48}=0$$

$$E_{55}=\iint_A Q_{66}^* n^2 dnds,\quad E_{56}=\iint_A Q_{66}^* n\cos\varphi_s dnds$$

$$E_{57}=\iint_A Q_{66}^* n\sin\varphi_s dnds,\quad E_{58}=\iint_A Q_{66}^* nrdnds,\quad E_{66}=\iint_A\left(Q_{66}^*\cos^2\varphi_s+Q_{55}^*\sin^2\varphi_s\right)dnds$$

$$E_{67}=\iint_A\left(Q_{66}^*-Q_{55}^*\right)\sin\varphi_s\cos\varphi_s dnds,\quad E_{68}=\iint_A\left(Q_{66}^* r\cos\varphi_s-Q_{55}^* q\sin\varphi_s\right)dnds$$

$$E_{77}=\iint_A\left(Q_{66}^*\sin^2\varphi_s+Q_{55}^*\cos^2\varphi_s\right)dnds,\quad E_{78}=\iint_A\left(Q_{66}^* r\sin\varphi_s+Q_{55}^* q\cos\varphi_s\right)dnds$$

$$E_{88}=\iint_A\left(Q_{66}^* r^2+Q_{55}^* q^2\right)dnds \tag{A1}$$

Appendix B: Matrix **K** and Vetor **F**

$$K_{ij}^{11} = E_{11}\int_0^L \zeta_i^{"}\zeta_j^{"}dx, \quad K_{ij}^{12} = -E_{12}\int_0^L \zeta_i^{"}\zeta_j^{"}dx, \quad K_{ij}^{13} = -E_{13}\int_0^L \zeta_i^{"}\zeta_j^{"}dx,$$

$$K_{ij}^{14} = -E_{14}\int_0^L \zeta_i^{"}\zeta_j^{"}dx + 2E_{15}\int_0^L \zeta_i^{"}\zeta_j^{'}dx,$$

$$K_{ij}^{15} = E_{16}\int_0^L \zeta_i^{"}\zeta_j^{'}dx, \quad K_{ij}^{16} = E_{17}\int_0^L \zeta_i^{"}\zeta_j^{'}dx,$$

$$K_{ij}^{17} = \left(E_{15}+E_{18}\right)\int_0^L \zeta_i^{"}\zeta_j^{'}dx \quad , \qquad K_{ij}^{22} = E_{22}\int_0^L \zeta_i^{"}\zeta_j^{"}dx + k_y\int_0^L \zeta_i\zeta_j dx + g_y\int_0^L \zeta_i^{'}\zeta_j^{'}dx + N_0\int_0^L \zeta_i^{'}\zeta_j^{'}dx \quad ,$$

$$K_{ij}^{23} = E_{23}\int_0^L \zeta_i^{"}\zeta_j^{"}dx,$$

$$K_{ij}^{24} = E_{24}\int_0^L \zeta_i^{"}\zeta_j^{"}dx - 2E_{25}\int_0^L \zeta_i^{"}\zeta_j^{'}dx - k_y\left(l_y - y_P\right)\int_0^L \zeta_i\zeta_j dx - g_y\left(l_y - y_P\right)\int_0^L \zeta_i^{'}\zeta_j^{'}dx + z_P N_0\int_0^L \zeta_i^{'}\zeta_j^{'}dx \ ,$$

$$K_{ij}^{25} = -E_{26}\int_0^L \zeta_i^{"}\zeta_j^{'}dx + k_y\int_0^L \zeta_i\zeta_j dx + g_y\int_0^L \zeta_i^{'}\zeta_j^{'}dx + N_0\int_0^L \zeta_i^{'}\zeta_j^{'}dx, K_{ij}^{26} = -E_{27}\int_0^L \zeta_i^{"}\zeta_j^{'}dx,$$

$$K_{ij}^{27} = -\left(E_{25}+E_{28}\right)\int_0^L \zeta_i^{"}\zeta_j^{'}dx - k_y\left(l_y - y_P\right)\int_0^L \zeta_i\zeta_j dx - g_y\left(l_y - y_P\right)\int_0^L \zeta_i^{'}\zeta_j^{'}dx + z_P N_0\int_0^L \zeta_i^{'}\zeta_j^{'}dx,$$

$$K_{ij}^{33} = E_{33}\int_0^L \zeta_i^{"}\zeta_j^{"}dx + k_z\int_0^L \zeta_i\zeta_j dx + g_z\int_0^L \zeta_i^{'}\zeta_j^{'}dx + N_0\int_0^L \zeta_i^{'}\zeta_j^{'}dx,$$

$$K_{ij}^{34} = E_{34}\int_0^L \zeta_i^{"}\zeta_j^{"}dx - 2E_{35}\int_0^L \zeta_i^{"}\zeta_j^{'}dx + k_z\left(l_z - z_P\right)\int_0^L \zeta_i\zeta_j dx + g_z\left(l_z - z_P\right)\int_0^L \zeta_i^{'}\zeta_j^{'}dx - y_P N_0\int_0^L \zeta_i^{'}\zeta_j^{'}dx,$$

$$K_{ij}^{35} = -E_{36}\int_0^L \zeta_i^{"}\zeta_j^{'}dx, \quad K_{ij}^{36} = -E_{37}\int_0^L \zeta_i^{"}\zeta_j^{'}dx + k_z\int_0^L \zeta_i\zeta_j dx + g_z\int_0^L \zeta_i^{'}\zeta_j^{'}dx + N_0\int_0^L \zeta_i^{'}\zeta_j^{'}dx,$$

$$K_{ij}^{37} = -\left(E_{35}+E_{38}\right)\int_0^L \zeta_i^{"}\zeta_j^{'}dx + k_z\left(l_z - z_P\right)\int_0^L \zeta_i\zeta_j dx + g_z\left(l_z - z_P\right)\int_0^L \zeta_i^{'}\zeta_j^{'}dx - y_P N_0\int_0^L \zeta_i^{'}\zeta_j^{'}dx,$$

$$K_{ij}^{44}=E_{44}\int_0^L\zeta_i''\zeta_j''dx-4E_{45}\int_0^L\zeta_i''\zeta_j'dx+4E_{55}\int_0^L\zeta_i'\zeta_j'dx+k_y\left(l_y-y_P\right)^2\int_0^L\zeta_i\zeta_j dx+g_y\left(l_y-y_P\right)^2\int_0^L\zeta_i'\zeta_j'dx$$

$$+k_z\left(l_z-z_P\right)^2\int_0^L\zeta_i\zeta_j dx+g_z\left(l_z-z_P\right)^2\int_0^L\zeta_i'\zeta_j'dx+k_t\int_0^L\zeta_i\zeta_j dx+\frac{I_P N_0}{A}\int_0^L\zeta_i'\zeta_j'dx,$$

$$K_{ij}^{45}=-E_{46}\int_0^L\zeta_i''\zeta_j'dx+2E_{56}\int_0^L\zeta_i'\zeta_j'dx-k_y\left(l_y-y_P\right)\int_0^L\zeta_i\zeta_j dx-g_y\left(l_y-y_P\right)\int_0^L\zeta_i'\zeta_j'dx+z_P N_0\int_0^L\zeta_i'\zeta_j'dx,$$

$$K_{ij}^{46}=-E_{47}\int_0^L\zeta_i''\zeta_j'dx+2E_{57}\int_0^L\zeta_i'\zeta_j'dx+k_z\left(l_z-z_P\right)\int_0^L\zeta_i\zeta_j dx+g_z\left(l_z-z_P\right)\int_0^L\zeta_i'\zeta_j'dx-y_P N_0\int_0^L\zeta_i'\zeta_j'dx,$$

$$K_{ij}^{47}=-\left(E_{45}+E_{48}\right)\int_0^L\zeta_i''\zeta_j'dx+2\left(E_{55}+E_{88}\right)\int_0^L\zeta_i'\zeta_j'dx+k_y\left(l_y-y_P\right)^2\int_0^L\zeta_i\zeta_j dx+g_y\left(l_y-y_P\right)^2\int_0^L\zeta_i'\zeta_j'dx$$

$$+k_z\left(l_z-z_P\right)^2\int_0^L\zeta_i\zeta_j dx+g_z\left(l_z-z_P\right)^2\int_0^L\zeta_i'\zeta_j'dx+k_t\int_0^L\zeta_i\zeta_j dx+\frac{I_P N_0}{A}\int_0^L\zeta_i'\zeta_j'dx$$

$$K_{ij}^{55}=E_{66}\int_0^L\zeta_i'\zeta_j'dx+k_y\int_0^L\zeta_i\zeta_j dx+g_y\int_0^L\zeta_i'\zeta_j'dx+N_0\int_0^L\zeta_i'\zeta_j'dx\,,$$

$$K_{ij}^{56}=E_{67}\int_0^L\zeta_i'\zeta_j'dx,$$

$$K_{ij}^{57}=\left(E_{56}+E_{68}\right)\int_0^L\zeta_i'\zeta_j'dx-k_y\left(l_y-y_P\right)\int_0^L\zeta_i\zeta_j dx-g_y\left(l_y-y_P\right)\int_0^L\zeta_i'\zeta_j'dx+z_P N_0\int_0^L\zeta_i'\zeta_j'dx,$$

$$K_{ij}^{66}=E_{77}\int_0^L\zeta_i'\zeta_j'dx+k_z\int_0^L\zeta_i\zeta_j dx+g_z\int_0^L\zeta_i'\zeta_j'dx+N_0\int_0^L\zeta_i'\zeta_j'dx\,,$$

$$K_{ij}^{67}=\left(E_{57}+E_{78}\right)\int_0^L\zeta_i'\zeta_j'dx+k_z\left(l_z-z_P\right)\int_0^L\zeta_i\zeta_j dx+g_z\left(l_z-z_P\right)\int_0^L\zeta_i'\zeta_j'dx-y_P N_0\int_0^L\zeta_i'\zeta_j'dx,$$

$$K_{ij}^{77}=\left(E_{55}+2E_{58}+E_{88}\right)\int_0^L\zeta_i'\zeta_j'dx+k_y\left(l_y-y_P\right)^2\int_0^L\zeta_i\zeta_j dx+g_y\left(l_y-y_P\right)^2\int_0^L\zeta_i'\zeta_j'dx$$

$$+k_z\left(l_z-z_P\right)^2\int_0^L\zeta_i\zeta_j dx+g_z\left(l_z-z_P\right)^2\int_0^L\zeta_i'\zeta_j'dx+k_t\int_0^L\zeta_i\zeta_j dx+\frac{I_P N_0}{A}\int_0^L\zeta_i'\zeta_j'dx$$

$$F_{bi}=\int_0^L q_z\zeta_j dx+P_z\zeta_j\left(x_L\right)\quad,\quad F_{si}=\int_0^L q_z\zeta_j dx+P_z\zeta_j\left(x_L\right)\qquad\text{(B1)}$$

References

1. V. Birman and G.A. Kardomateas, Review of current trends in research and applications of sandwich structures, *Composites Part B: Engineering*. **142** (2018) 221-240.
2. A.S. Sayyad and Y.M. Ghugal, Modeling and analysis of functionally graded sandwich beams: A review, *Mechanics of Advanced Materials and Structures*. **26**(21) (2019) 1776-1795.
3. V. Vlasov, *Thin-walled elastic beams. Israel program for scientific translations, Jerusalem*. 1961, Oldbourne Press, London.
4. N.-I. Kim and J. Lee, Refined Series Methodology for the Fully Coupled Thin-Walled Laminated Beams Considering Foundation Effects, *Mechanics Based Design of Structures and Machines*. **43**(2) (2015) 125-149.
5. J. Lee and S.-E. Kim, Flexural–torsional buckling of thin-walled I-section composites, *Computers & Structures*. **79**(10) (2001) 987-995.
6. J. Lee, Center of gravity and shear center of thin-walled open-section composite beams, *Composite structures*. **52**(2) (2001) 255-260.
7. N.R. Bauld and T. Lih-Shyng, A Vlasov theory for fiber-reinforced beams with thin-walled open cross sections, *International Journal of Solids and Structures*. **20**(3) (1984) 277-297.
8. T.-T. Nguyen, N.-I. Kim, and J. Lee, Analysis of thin-walled open-section beams with functionally graded materials, *Composite Structures*. **138** (2016) 75-83.
9. N.-I. Kim and J. Lee, Exact solutions for coupled responses of thin-walled FG sandwich beams with non-symmetric cross-sections, *Composites Part B: Engineering*. **122** (2017) 121-135.

10. N.-I. Kim and J. Lee, Theory of thin-walled functionally graded sandwich beams with single and double-cell sections, *Composite Structures*. **157** (2016) 141-154.
11. D. Lanc, G. Turkalj, T.P. Vo, and J. Brnić, Nonlinear buckling behaviours of thin-walled functionally graded open section beams, *Composite Structures*. **152** (2016) 829-839.
12. L. Librescu, S.Y. Oh, and O. Song, Spinning thin-walled beams made of functionally graded materials: modeling, vibration and instability, *European Journal of Mechanics-A/Solids*. **23**(3) (2004) 499-515.
13. T.-T. Nguyen, P.T. Thang, and J. Lee, Flexural-torsional stability of thin-walled functionally graded open-section beams, *Thin-Walled Structures*. **110** (2017) 88-96.
14. T.-T. Nguyen, P.T. Thang, and J. Lee, Lateral buckling analysis of thin-walled functionally graded open-section beams, *Composite Structures*. **160** (2017) 952-963.
15. D. Lanc, T.P. Vo, G. Turkalj, and J. Lee, Buckling analysis of thin-walled functionally graded sandwich box beams, *Thin-Walled Structures*. **86** (2015) 148-156.
16. N.-I. Kim and J. Lee, Flexural-torsional analysis of functionally graded sandwich I-beams considering shear effects, *Composites Part B: Engineering*. **108** (2017) 436-450.
17. J. Lee, Flexural analysis of thin-walled composite beams using shear-deformable beam theory, *Composite Structures*. **70**(2) (2005) 212-222.
18. N.-I. Kim and J. Lee, Investigation of coupled instability for shear flexible FG sandwich I-beams subjected to variable axial force, *Acta Mechanica*. **229**(1) (2018) 47-70.
19. M.D. Demirbas, U. Caliskan, X. Xu, and M. Filippi, Evaluation of the bending

response of compact and thin-walled FG beams with CUF, *Mechanics of Advanced Materials and Structures* (2020) 1-10.

20. S. Kvaternik, M. Filippi, D. Lanc, G. Turkalj, and E. Carrera, Comparison of classical and refined beam models applied on isotropic and FG thin-walled beams in nonlinear buckling response, *Composite Structures*. **229** (2019) 111490.
21. M. Khiloun, A.A. Bousahla, A. Kaci, A. Bessaim, A. Tounsi, and S. Mahmoud, Analytical modeling of bending and vibration of thick advanced composite plates using a four-variable quasi 3D HSDT, *Engineering with Computers*. **36**(3) (2020) 807-821.
22. A. Boussoula, B. Boucham, M. Bourada, F. Bourada, A. Tounsi, A.A. Bousahla, and A. Tounsi, A simple nth-order shear deformation theory for thermomechanical bending analysis of different configurations of FG sandwich plates, *Smart Structures and Systems*. **25**(2) (2020) 197-218.
23. M. Balubaid, A. Tounsi, B. Dakhel, and S. Mahmoud, Free vibration investigation of FG nanoscale plate using nonlocal two variables integral refined plate theory, *Computers and Concrete*. **24**(6) (2019) 579-586.
24. B. Karami, M. Janghorban, and A. Tounsi, Galerkin's approach for buckling analysis of functionally graded anisotropic nanoplates/different boundary conditions, *Engineering with Computers*. **35**(4) (2019) 1297-1316.
25. M. Hussain, M.N. Naeem, M.S. Khan, and A. Tounsi, Computer-aided approach for modelling of FG cylindrical shell sandwich with ring supports, *Computers and Concrete*. **25**(5) (2020) 411-425.
26. H.-T. Thai and D.-H. Choi, A simple first-order shear deformation theory for the bending and free vibration analysis of functionally graded plates, *Composite*

Structures. **101** (2013) 332-340.

27. H.-T. Thai and D.-H. Choi, A simple first-order shear deformation theory for laminated composite plates, *Composite Structures*. **106** (2013) 754-763.
28. H.-T. Thai, T.-K. Nguyen, T.P. Vo, and J. Lee, Analysis of functionally graded sandwich plates using a new first-order shear deformation theory, *European Journal of Mechanics-A/Solids*. **45** (2014) 211-225.
29. H.-T. Thai and D.-H. Choi, A refined plate theory for functionally graded plates resting on elastic foundation, *Composites Science and Technology*. **71**(16) (2011) 1850-1858.
30. S.-E. Kim, H.-T. Thai, and J. Lee, Buckling analysis of plates using the two variable refined plate theory, *Thin-Walled Structures*. **47**(4) (2009) 455-462.
31. T.P. Vo and H.-T. Thai, A new sinusoidal shear deformation theory for bending, buckling, and vibration of functionally graded plates, Applied mathematical modelling 37 (5) (2013) 3269-3281.
32. A. Karamanli, Bending behaviour of two directional functionally graded sandwich beams by using a quasi-3d shear deformation theory, Composite Structures 174, 2017, 70-86
33. T.P. Vo and H.-T. Thai, Bending and free vibration of functionally graded beams using various higher-order shear deformation beam theories, International Journal of Mechanical Sciences 62 (1) (2012) 57-66.
34. T.P. Vo and H.-T. Thai, T-K Nguyen, A. Maheri, J. Lee, Finite element model for vibration and buckling of functionally graded sandwich beams based on a refined shear deformation theory, Engineering Structures 64 (2014) 12-22.
35. T.P. Vo and H.-T. Thai, T-K Nguyen, F Inam, Static and vibration analysis of

functionally graded beams using refined shear deformation theory, Meccanica 49 (1) (2014) 155-168.

36. A. Karamanlı, T.P. Vo, Size dependent bending analysis of two directional functionally graded microbeams via a quasi-3D theory and finite element method, Composites Part B: Engineering 144, 2018, 171-183
37. S.C. Dutta and R. Roy, A critical review on idealization and modeling for interaction among soil–foundation–structure system, *Computers & structures*. **80**(20-21) (2002) 1579-1594.
38. Q.L. Li and Q.H. Shao, Non-linear analysis of a FGM cantilever beam supported on a winkler elastic foundation, *Applied Mechanics and Materials*. (2014), (131-134).
39. Ş.D. Akbaş, Free vibration and bending of functionally graded beams resting on elastic foundation, *Research on Engineering Structures and Materials*. **1**(1) (2015) 25-37.
40. B.S. Gan and N.D. Kien, Large deflection analysis of functionally graded beams resting on a two-parameter elastic foundation, *Journal of Asian Architecture and Building Engineering*. **13**(3) (2014) 649-656.
41. J. Ying, C. Lü, and W. Chen, Two-dimensional elasticity solutions for functionally graded beams resting on elastic foundations, *Composite Structures*. **84**(3) (2008) 209-219.
42. I. Esen, Dynamic response of a functionally graded Timoshenko beam on two-parameter elastic foundations due to a variable velocity moving mass, *International Journal of Mechanical Sciences*. **153** (2019) 21-35.
43. B. Fahsi, R.B. Bouiadjra, A. Mahmoudi, S. Benyoucef, and A. Tounsi, Assessing the Effects of Porosity on the Bending, Buckling, and Vibrations of Functionally

Graded Beams Resting on an Elastic Foundation by Using a New Refined Quasi-3D Theory, *Mechanics of Composite Materials*. **55**(2) (2019) 219-230.

44. L.A. Chaabane, F. Bourada, M. Sekkal, S. Zerouati, F.Z. Zaoui, A. Tounsi, A. Derras, A.A. Bousahla, and A. Tounsi, Analytical study of bending and free vibration responses of functionally graded beams resting on elastic foundation, *Structural Engineering and Mechanics*. **71**(2) (2019) 185-196.
45. H. Matouk, A.A. Bousahla, H. Heireche, F. Bourada, E. Bedia, A. Tounsi, S. Mahmoud, A. Tounsi, and K. Benrahou, Investigation on hygro-thermal vibration of P-FG and symmetric S-FG nanobeam using integral Timoshenko beam theory, *Advances in nano research*. **8**(4) (2020) 293-305.
46. A.A. Bousahla, F. Bourada, S. Mahmoud, A. Tounsi, A. Algarni, E. Bedia, and A. Tounsi, Buckling and dynamic behavior of the simply supported CNT-RC beams using an integral-first shear deformation theory, *Computers and Concrete*. **25**(2) (2020) 155-166.
47. F. Bourada, A.A. Bousahla, A. Tounsi, E. Bedia, S. Mahmoud, K.H. Benrahou, and A. Tounsi, Stability and dynamic analyses of SW-CNT reinforced concrete beam resting on elastic-foundation, *Computers and Concrete*. **25**(6) (2020) 485-495.
48. M. Rabhi, K.H. Benrahou, A. Kaci, M.S.A. Houari, F. Bourada, A.A. Bousahla, A. Tounsi, E.A. Bedia, S. Mahmoud, and A. Tounsi, A new innovative 3-unknowns HSDT for buckling and free vibration of exponentially graded sandwich plates resting on elastic foundations under various boundary conditions, *Geomechanics and Engineering*. **22**(2) (2020) 119.
49. S.C. Chikr, A. Kaci, A.A. Bousahla, F. Bourada, A. Tounsi, E. Bedia, S. Mahmoud, K.H. Benrahou, and A. Tounsi, A novel four-unknown integral model for buckling

response of FG sandwich plates resting on elastic foundations under various boundary conditions using Galerkin's approach, *Geomechanics and Engineering*. **21**(5) (2020) 471-487.

50. M. Kaddari, A. Kaci, A.A. Bousahla, A. Tounsi, F. Bourada, A. Tounsi, E. Bedia, and M.A. Al-Osta, A study on the structural behaviour of functionally graded porous plates on elastic foundation using a new quasi-3D model: Bending and free vibration analysis, *Computers and Concrete*. **25**(1) (2020) 37-57.
51. M.C. Rahmani, A. Kaci, A.A. Bousahla, F. Bourada, A. Tounsi, E. Bedia, S. Mahmoud, K.H. Benrahou, and A. Tounsi, Influence of boundary conditions on the bending and free vibration behavior of FGM sandwich plates using a four-unknown refined integral plate theory, *Computers and Concrete*. **25**(3) (2020) 225-244.
52. S. Refrafi, A.A. Bousahla, A. Bouhadra, A. Menasria, F. Bourada, A. Tounsi, E. Bedia, S. Mahmoud, K.H. Benrahou, and A. Tounsi, Effects of hygro-thermo-mechanical conditions on the buckling of FG sandwich plates resting on elastic foundations, *Computers and Concrete*. **25**(4) (2020) 311-325.
53. A. Tounsi, S. Al-Dulaijan, M.A. Al-Osta, A. Chikh, M. Al-Zahrani, A. Sharif, and A. Tounsi, A four variable trigonometric integral plate theory for hygro-thermo-mechanical bending analysis of AFG ceramic-metal plates resting on a two-parameter elastic foundation, *Steel and Composite Structures*. **34**(4) (2020) 511.
54. A. Shariati, A. Ghabussi, M. Habibi, H. Safarpour, M. Safarpour, A. Tounsi, and M. Safa, Extremely large oscillation and nonlinear frequency of a multi-scale hybrid disk resting on nonlinear elastic foundation, *Thin-Walled Structures*. **154** (2020) 106840.
55. M. Al-Furjan, H. Safarpour, M. Habibi, M. Safarpour, and A. Tounsi, A

comprehensive computational approach for nonlinear thermal instability of the electrically FG-GPLRC disk based on GDQ method, *Engineering with Computers* (2020) 1-18.

56. N.-I. Kim and J. Lee, Nonlinear analysis of thin-walled Al/Al2O3 FG sandwich I-beams with mono-symmetric cross-section, *European Journal of Mechanics-A/Solids*. **69** (2018) 55-70.
57. T.-T. Nguyen and J. Lee, Optimal design of thin-walled functionally graded beams for buckling problems, *Composite Structures*. **179** (2017) 459-467.
58. F.A. Fazzolari, Quasi-3D beam models for the computation of eigenfrequencies of functionally graded beams with arbitrary boundary conditions, *Composite Structures*. **154** (2016) 239-255.
59. D. Chen, J. Yang, and S. Kitipornchai, Free and forced vibrations of shear deformable functionally graded porous beams, *International journal of mechanical sciences*. **108** (2016) 14-22.
60. K. Pradhan and S. Chakraverty, Free vibration of Euler and Timoshenko functionally graded beams by Rayleigh–Ritz method, *Composites Part B: Engineering*. **51** (2013) 175-184.
61. N. Wattanasakulpong, B.G. Prusty, and D.W. Kelly, Thermal buckling and elastic vibration of third-order shear deformable functionally graded beams, *International Journal of Mechanical Sciences*. **53**(9) (2011) 734-743.
62. M. Şimşek, Static analysis of a functionally graded beam under a uniformly distributed load by Ritz method, *International Journal of Engineering and Applied Sciences*. **1**(3) (2009) 1-11.
63. N.-D. Nguyen, T.-K. Nguyen, T.P. Vo, T.-N. Nguyen, and S. Lee, Vibration and

buckling behaviours of thin-walled composite and functionally graded sandwich I-beams, *Composites Part B: Engineering*. **166** (2019) 414-427.

64. N.-I. Kim, Shear deformable composite beams with channel-section on elastic foundation, *European Journal of Mechanics-A/Solids*. **36** (2012) 104-121.
65. G. Dube and P. Dumir, Tapered thin open section beams on elastic foundation—I. Buckling analysis, *Computers & structures*. **61**(5) (1996) 845-857.

Figure Captions

Figure 1. Coordinate systems of thin-walled beam

Figure 2. Thin-walled FG sandwich I-beam.

Figure 3. Coordinate and foundation parameters of FG I-beams

Figure 4. Variation of the shear effect respect to the length-to-height ratio of FG I-beams

Figure 5. Variation of the shear effect and E_{33}/E_{77} ratio of the FG I-beams ($\alpha_3 = 0.1$) respect to α_1 and α_2

Figure 6. Variation of the shear effect and E_{33}/E_{77} ratio of the

Figure 7. Variation of the shear effect and E_{33}/E_{77} ratio of the

Figure 8. Thin-walled FG I-beam resting on the foundation.

Figure 9. Variation of transverse deflection of C-C and C-S FG I-beams along their span

Figure 10. The effect of the first foundation parameter on the mid-span deflections of the FG I-beams respect to the length-to-height ratio.

Figure 11. The effect of the second foundation parameter on the mid-spans deflection of the FG I-beams respect to the length-to-height ratio

Figure 12. Variation of first three buckling loads of FG I-beams ($\alpha_3 = 0.4$, p = 10, S1-section) respect to α_1, α_2

Figure 13. Variation of first three buckling loads of FG I-beams ($\alpha_1 = \alpha_2 = 0.7$, p = 10, S1-section) respect to α_3

Figure 14. The buckling mode 1 of FG C-S I-beam.

Figure 15. The buckling mode 2of FG C-S I-beam.

Figure 16. The buckling mode 3 of FG C-S I-beam.

Figure 17. The buckling mode 4 of FG C-S I-beam.

Figure 18. Variation of buckling loads of beams with S1-section respect to foundation parameters

Figure 19. Variation of buckling load of beams with S2-section respect to foundation parameters

Figure 20. Variation of r_f ration respect to length-to-height ratio

Table Captions

Table 1. Ritz's approximation functions for various boundary conditions (BCs).

Table 2. Convergence studies for deflections and buckling loads of FG I-beams

Table 3. Maximum deflection of isotropic simply supported I-beams subjected to the concentrated transverse load acting at mid-span (*mm*)

Table 4. Maximum deflections of cantilever FG I-beams ($h_1 = h_2 = h_3 = h = 0.002m$, $b_1 = 20h$, $b_2 = 10h$, $b_3 = 40h$, $L = 2.5m$, $\alpha_1 = 0.9$, $\alpha_2 = 0.1$, $\alpha_3 = 0.4$, S1-section) subjected to the concentrated transverse load at the free end.

Table 5. Maximum deflections of cantilever composite I-beams under the concentrated transverse load at the free end (*mm*)

Table 6. Mid-span deflections of FG I-beams subject to the concentrated transverse load acting at mid-span ($h_1 = h_2 = h_3 = h = 0.002m$, $b_1 = 20h$, $b_2 = 10h$, $b_3 = 40h$, $\alpha_1 = 0.9, \alpha_2 = 0.1, \alpha_3 = 0.4$, $P_z = 10kN$, S1-section) (*mm*)

Table 7. Mid-span deflections of FG I-beams subject to the concentrated transverse load acting at mid-span ($h_1 = h_2 = h_3 = h = 0.002m$, $b_1 = 20h$, $b_2 = 10h$, $b_3 = 40h$, $\alpha_1 = \alpha_2 = \alpha_3 = 0.1$, $P_z = 10kN$, S2-section) (*mm*)

Table 8. Mid-span deflections of FG I-beams subjected to a uniformed transverse load ($h_1 = h_2 = h_3 = h = 0.002m$, $b_1 = 20h$, $b_2 = 10h$, $b_3 = 40h$, $p = 10$ $q_z = 5kN/m, \alpha_1 = 0.9, \alpha_2 = 0.1, \alpha_3 = 0.4$, S1-section) (*mm*)

Table 9. Mid-span deflections (*W*) of FG I-beams subjected to a uniformed transverse load ($h_1 = h_2 = h_3 = h = 0.002m$, $b_1 = 20h$, $b_2 = 10h$, $b_3 = 40h$, $p = 10$ $q_z = 5kN/m, \alpha_1 = \alpha_2 = \alpha_3 = 0.1$, S2-section) (*mm*)

Table 10. Critical buckling loads (*kN*) of FG I-beams ($h_1 = h_2 = h_3 = h = 0.005m$, $b_1 = b_2 = 0.1m$, $b_3 = 0.2m$, $L = 2.5m$, $\alpha_1 = \alpha_2 = \alpha_3 = 0.4$, S2-section) with various boundary conditions

Table 11. Critical buckling loads (*kN*) of FG S-S I-beams ($h_1 = h_2 = h_3 = h = 0.005m$, $b_1 = b_2 = 0.1m$, $b_3 = 0.2m$, $L = 2.5m$, $\alpha_1 = \alpha_2 = 0.7$, $\alpha_3 = 0.4$, S1-section)

Table 12. Critical buckling loads (*kN*) of FG C-F I-beams ($h_1 = h_2 = h_3 = h = 0.005m$, $b_1 = b_2 = 0.1m$, $b_3 = 0.2m$, $L = 2.5m$, $\alpha_1 = \alpha_2 = 0.7$, $\alpha_3 = 0.4$, S1-section)

Table 13. Critical buckling loads (*kN*) of FG C-S I-beams ($h_1 = h_2 = h_3 = h = 0.005m$, $b_1 = b_2 = 0.1m$, $b_3 = 0.2m$, $L = 2.5m$, $\alpha_1 = \alpha_2 = 0.7$, $\alpha_3 = 0.4$, S1-section).

Table 14. Critical buckling loads (*kN*) of FG C-C I-beams ($h_1 = h_2 = h_3 = h = 0.005m$, $b_1 = b_2 = 0.1m$, $b_3 = 0.2m$, $L = 2.5m$, $\alpha_1 = \alpha_2 = 0.7$, $\alpha_3 = 0.4$, S1-section).

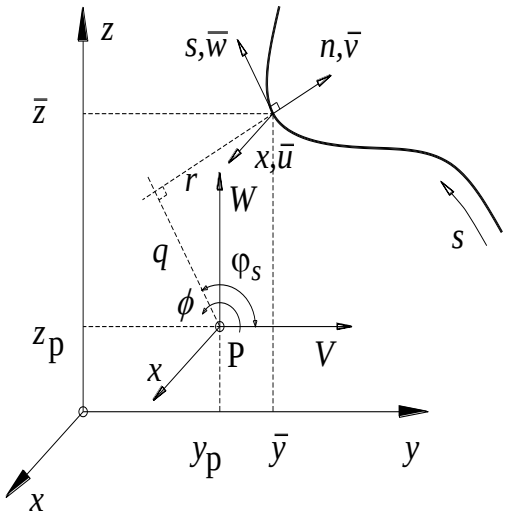

Figure 1. Coordinate systems of thin-walled beam

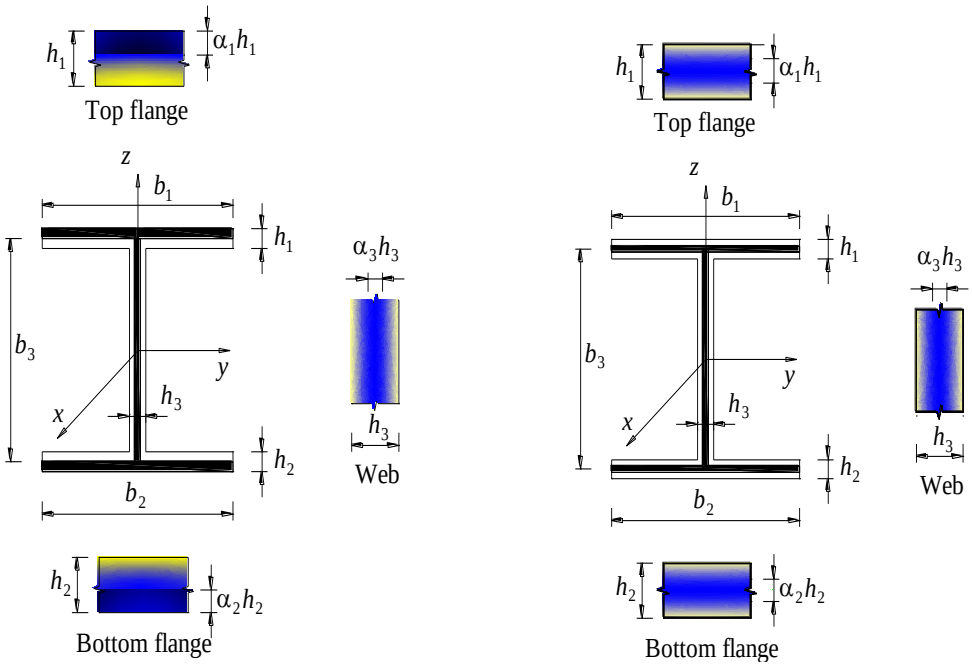

2a. S1-section 2b. S2-section

Figure 2. Thin-walled FG sandwich I-beam.

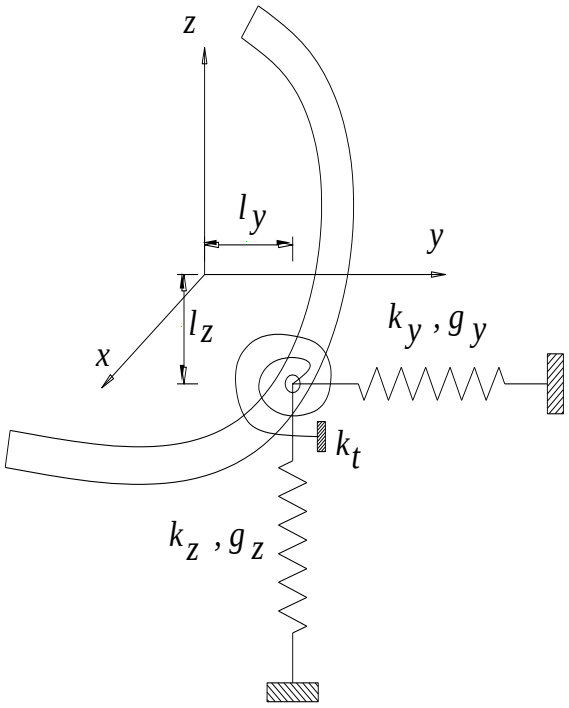

Figure 3. Coordinate and foundation parameters of FG I-beams

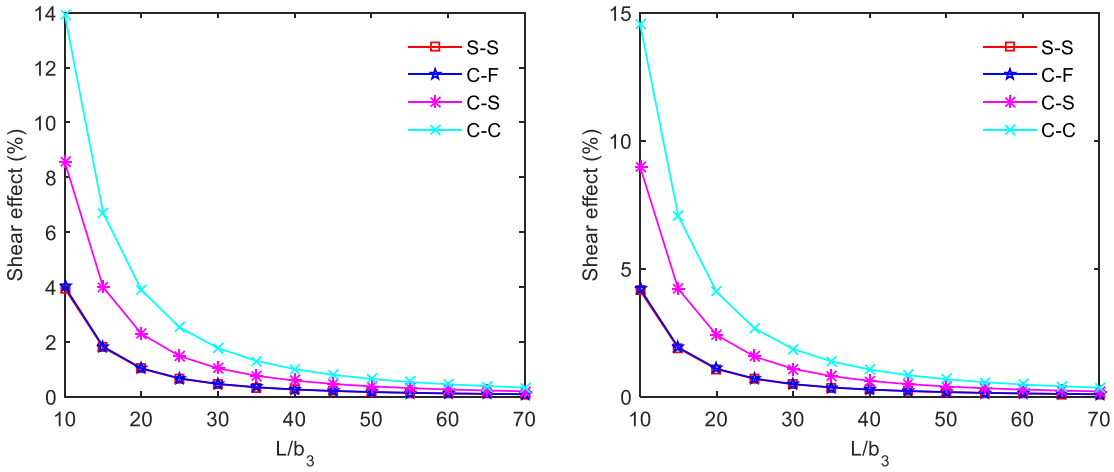

a. S1-section b. S2-section

Figure 4. Variation of the shear effect respect to the length-to-height ratio of FG I-beams

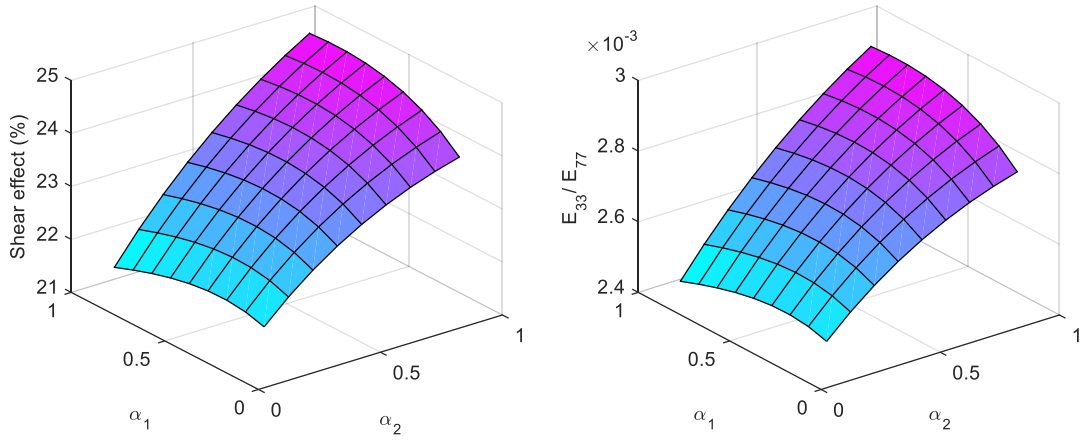

a. Shear effect (%) b. E_{33} / E_{77} ratio

Figure 5. Variation of the shear effect and E_{33} / E_{77} ratio of the FG I-beams ($\alpha_3 = 0.1$) respect to α_1 and α_2

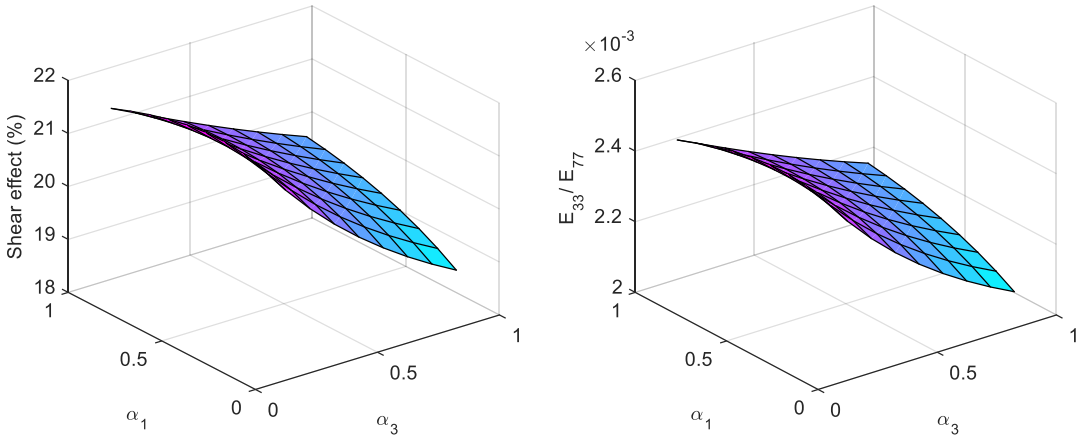

a. Shear effect (%) b. E_{33}/E_{77} ratio

Figure 6. Variation of the shear effect and E_{33}/E_{77} ratio of the FG I-beams ($\alpha_2 = 0.1$) respect to α_1 and α_3

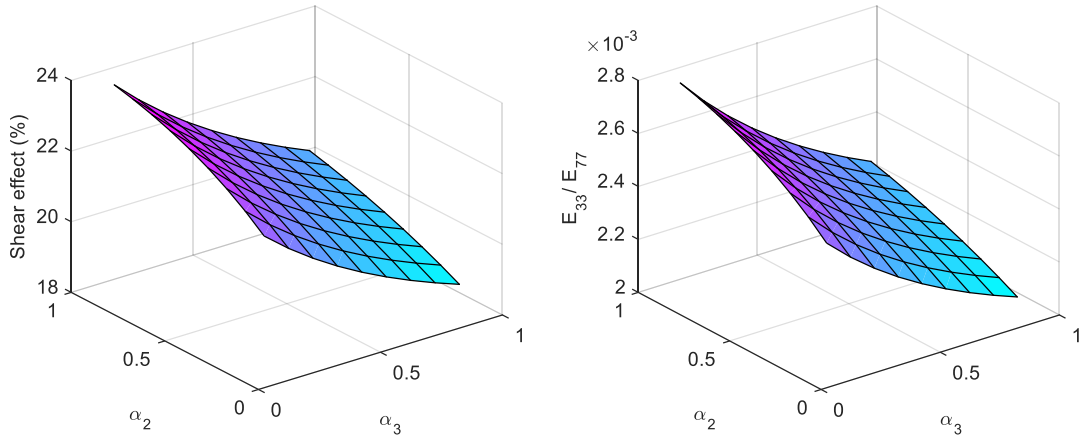

a. Shear effect (%) b. E_{33}/E_{77} ratio

Figure 7. Variation of the shear effect and E_{33}/E_{77} ratio of the FG I-beams ($\alpha_1 = 0.1$) respect to α_2 and α_3

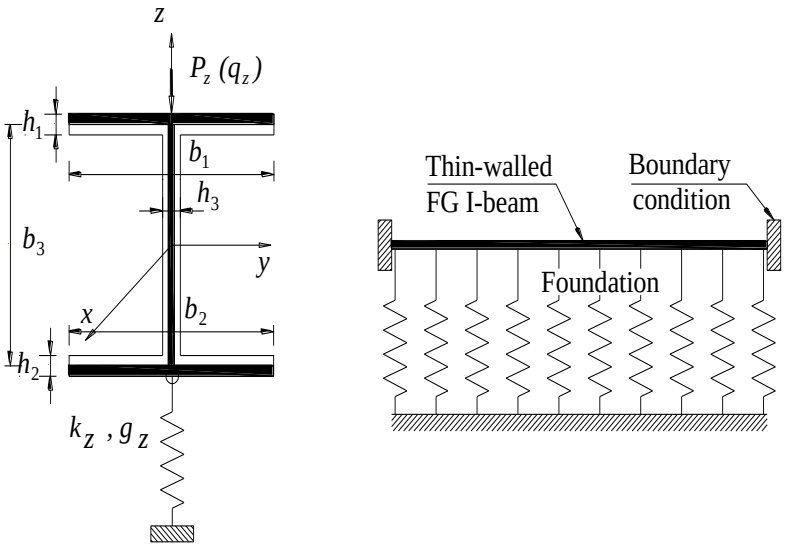

Figure 8. Thin-walled FG I-beam resting on the foundation.

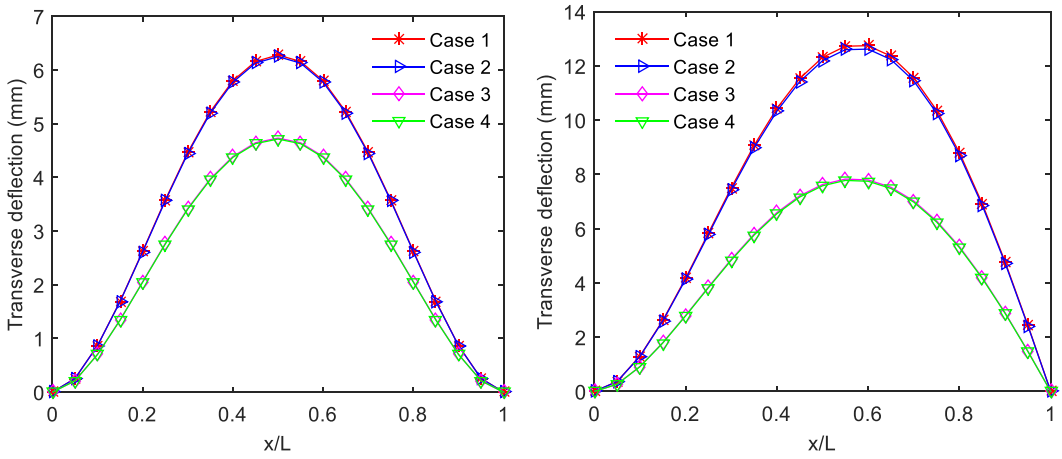

a. C-C beam b. C-S beam

Figure 9. Variation of transverse deflection of C-C and C-S FG I-beams along their span

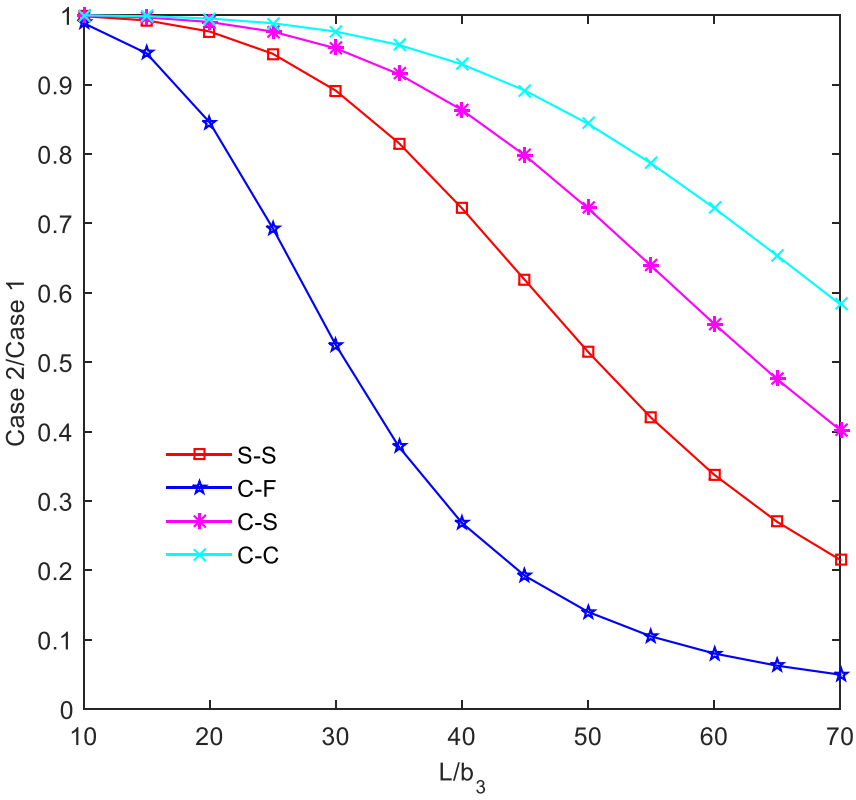

Figure 10. The effect of the first foundation parameter on the mid-span deflections of the FG I-beams respect to the length-to-height ratio.

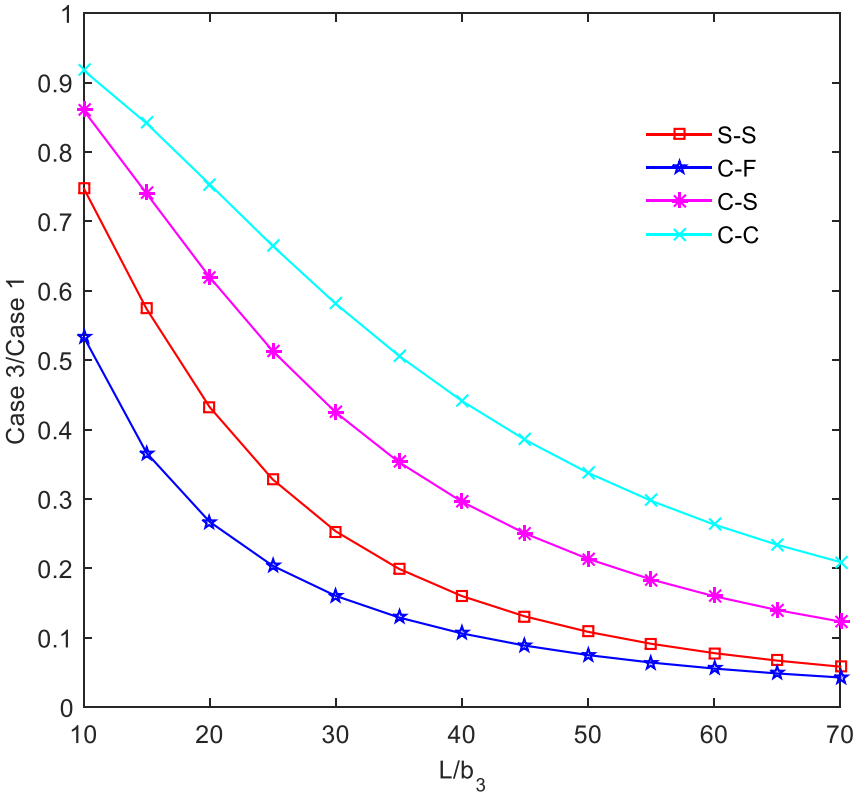

Figure 11. The effect of the second foundation parameter on the mid-spans deflection of the FG I-beams respect to the length-to-height ratio

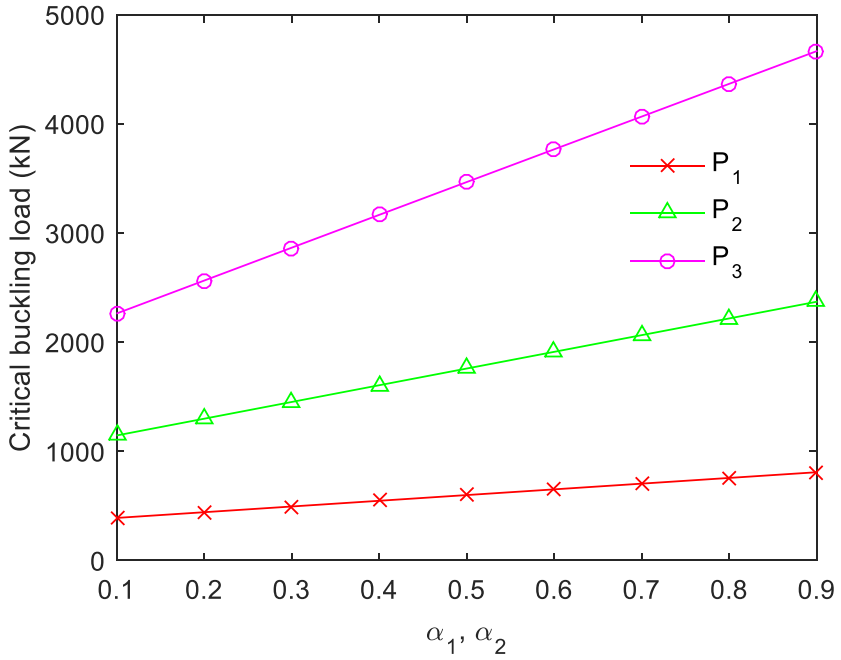

Figure 12. Variation of first three buckling loads of FG I-beams ($\alpha_3 = 0.4$, p = 10, S1-section) respect to α_1, α_2

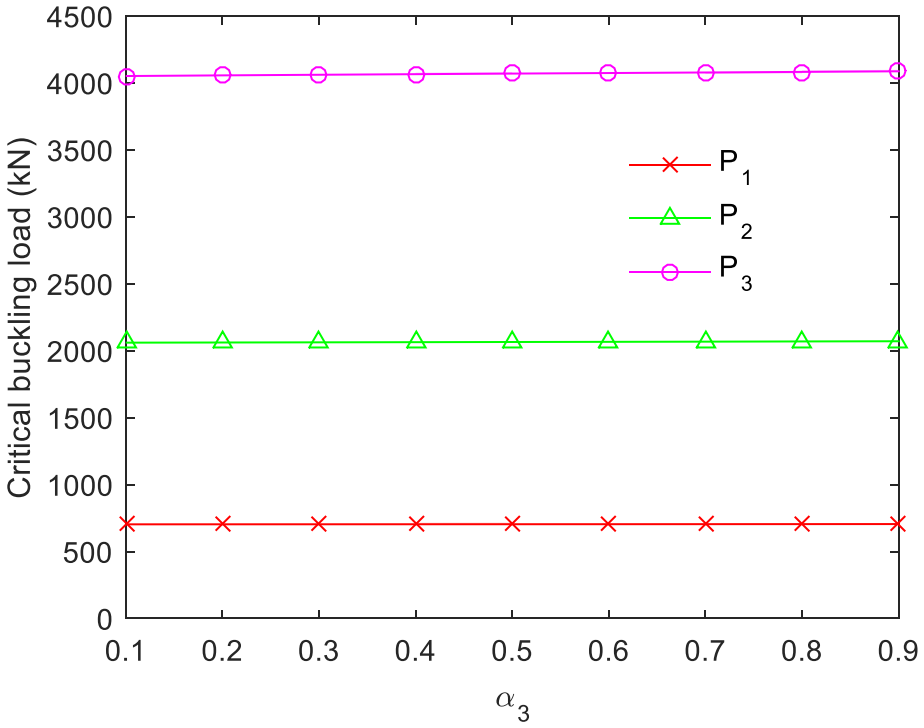

Figure 13. Variation of first three buckling loads of FG I-beams ($\alpha_1 = \alpha_2 = 0.7$, p = 10, S1-section) respect to α_3

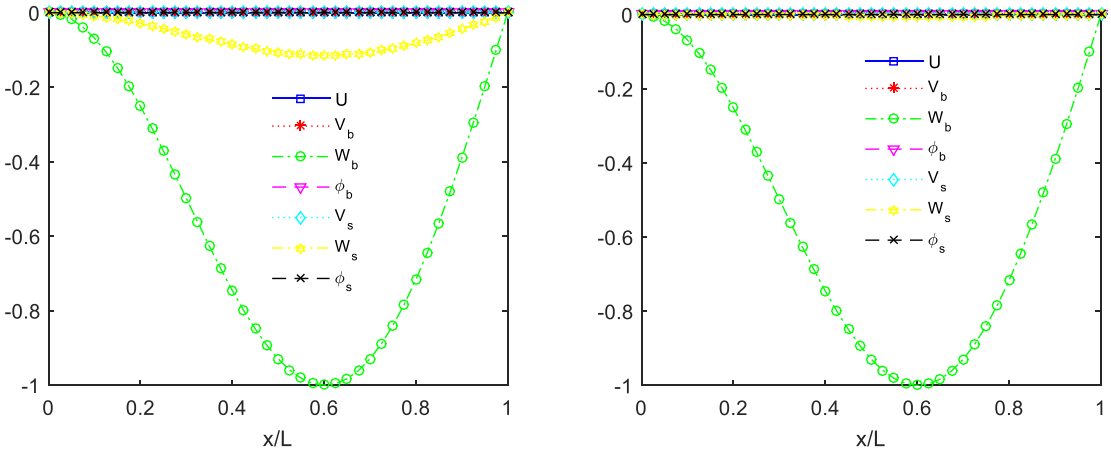

a. $P_1 = 10004.920\,kN\,(L/b_3 = 10)$ b. $P_1 = 443.780kN\ (L/b_3 = 50)$

Figure 14. The buckling mode 1 of FG C-S I-beam.

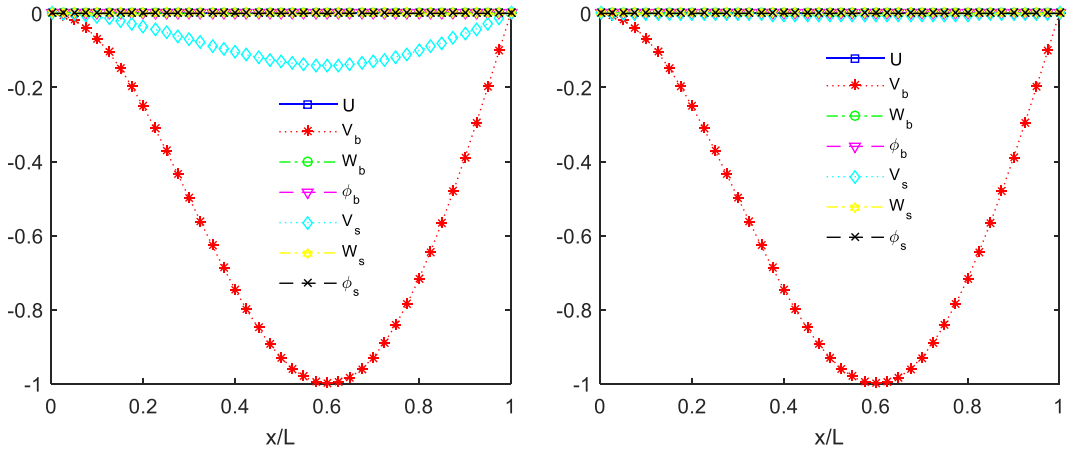

a. $P_2 = 12013.673kN$ $(L/b_3 = 10)$ b. $P_2 = 544.793kN$ $(L/b_3 = 50)$

Figure 15. The buckling mode 2of FG C-S I-beam.

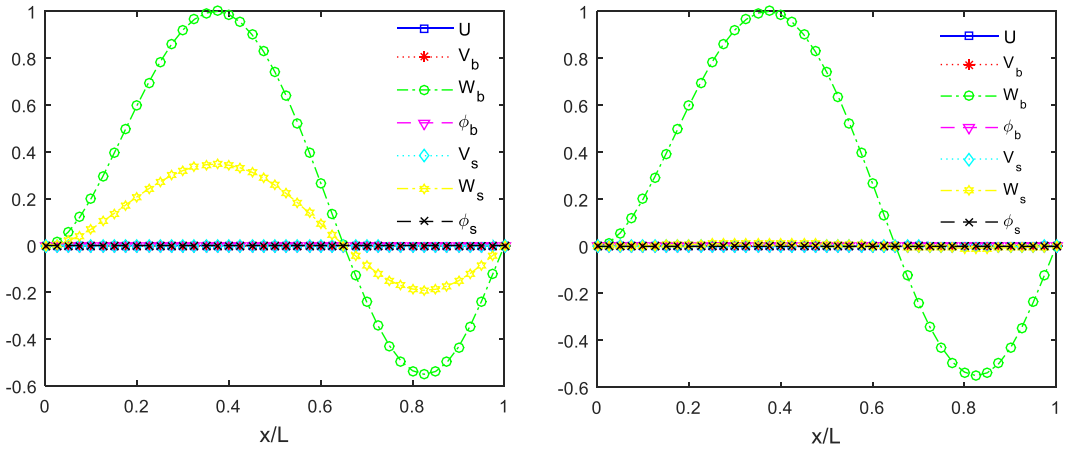

a. $P_3 = 24642.089 kN$ $(L/b_3 = 10)$ b. $P_3 = 1300.182 kN$ $(L/b_3 = 50)$

Figure 16. The buckling mode 3 of FG C-S I-beam.

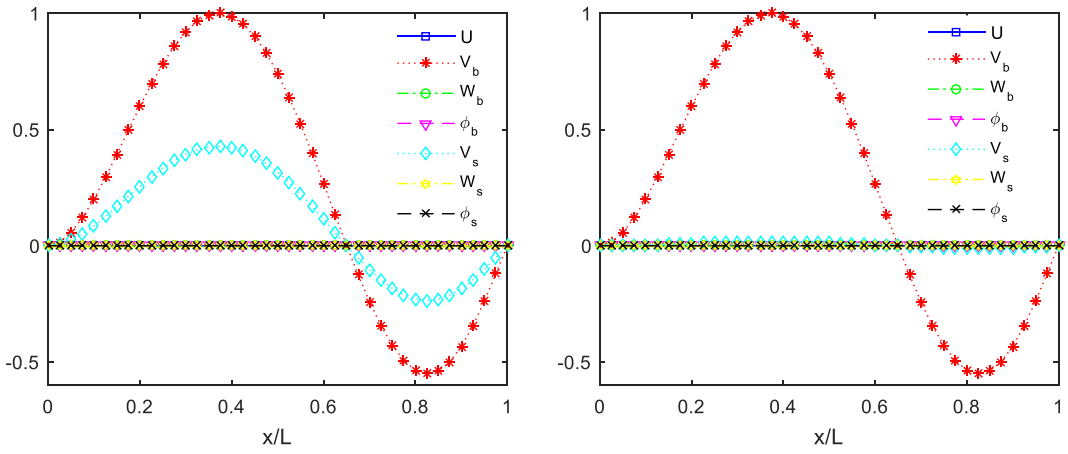

a. $P_4 = 28631.245 kN$ $(L/b_3 = 10)$ b. $P_4 = 1592.939 kN$ $(L/b_3 = 50)$

Figure 17. The buckling mode 4 of FG C-S I-beam.

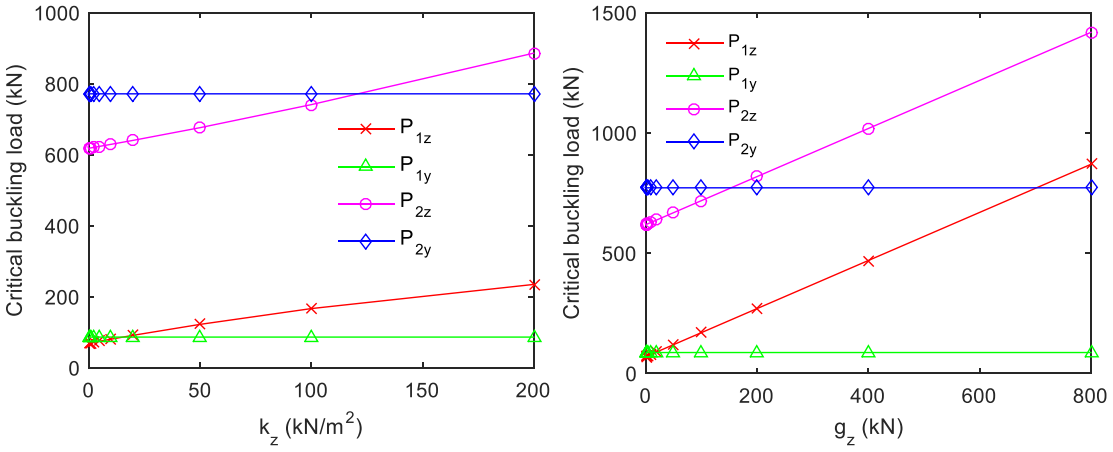

a. Critical buckling load respect to k_z b. Critical buckling load respect to g_z

Figure 18. Variation of buckling loads of beams with S1-section respect to foundation parameters

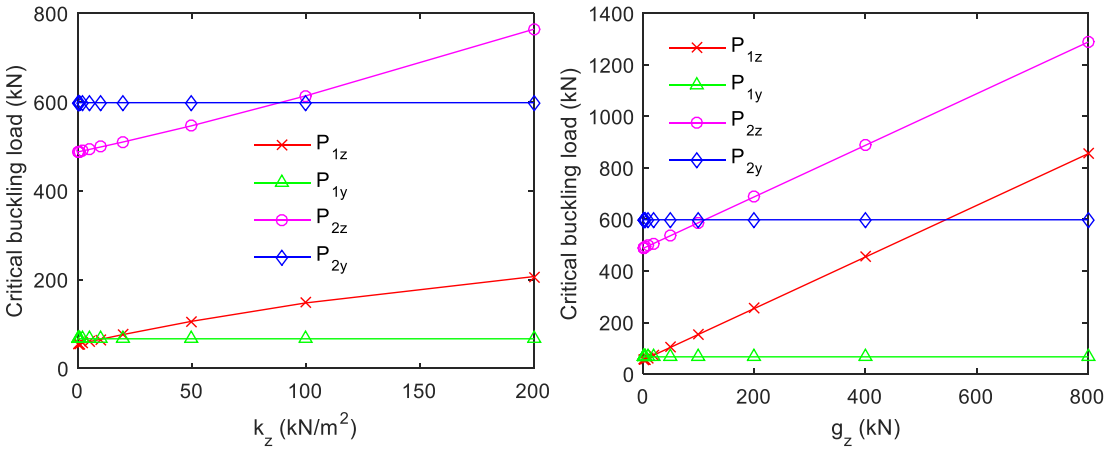

a. Critical buckling load respect to k_z b. Critical buckling load respect to g_z

Figure 19. Variation of buckling load of beams with S2-section respect to foundation parameters

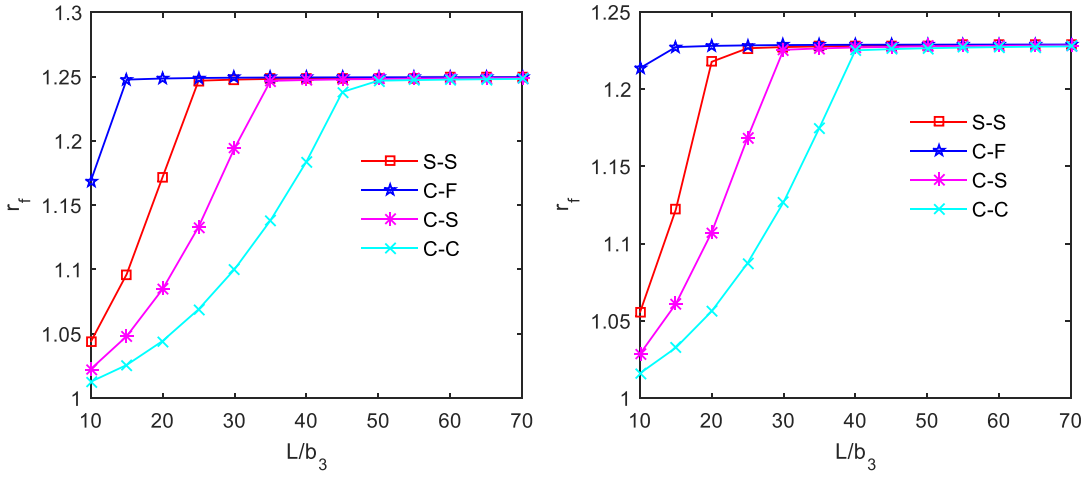

a. S1-section b. S2-section

Figure 20. Variation of r_f ration respect to length-to-height ratio

Table 1. Ritz's approximation functions for various boundary conditions (BCs).

BC	$\zeta_j(x)$	x=0	x=L
S-S	$\left(1-\frac{x}{L}\right)\frac{x}{L}e^{\frac{x}{j^2L}}$	$V_b=W_b=\phi_b=0$ $V_s=W_s=\phi_s=0$	$V_b=W_b=\phi_b=0$ $V_s=W_s=\phi_s=0$
C-F	$\left(\frac{x}{L}\right)^2 e^{\frac{x}{j^2L}}$	$U=V_b=W_b=\phi_b=0$ $V_s=W_s=\phi_s=0$ $V_b^{'}=W_b^{'}=V_s^{'}=W_s^{'}=0$	
C-S	$\left(1-\frac{x}{L}\right)\left(\frac{x}{L}\right)^2 e^{\frac{x}{j^2L}}$	$U=V_b=W_b=\phi_b=0$ $V_s=W_s=\phi_s=0$ $V_b^{'}=W_b^{'}=V_s^{'}=W_s^{'}=0$	$V_b=W_b=\phi_b=0$ $V_s=W_s=\phi_s=0$
C-C	$\left(1-\frac{x}{L}\right)^2\left(\frac{x}{L}\right)^2 e^{\frac{x}{j^2L}}$	$U=V_b=W_b=\phi_b=0$ $V_s=W_s=\phi_s=0$ $V_b^{'}=W_b^{'}=V_s^{'}=W_s^{'}=0$	$U=V_b=W_b=\phi_b=0$ $V_s=W_s=\phi_s=0$ $V_b^{'}=W_b^{'}=V_s^{'}=W_s^{'}=0$

Table 2. Convergence studies for deflections and buckling loads of FG I-beams

BC	Present	*m*					
		2	4	6	8	10	12
1. Deflection at mid-span (*mm*)							
S-S	With shear	8.081	9.778	9.897	9.928	9.940	9.940
	No shear	7.822	9.487	9.592	9.615	9.622	9.622
C-F	With shear	13.386	19.709	19.825	19.883	19.890	19.890
	No shear	13.118	19.116	19.221	19.244	19.251	19.251
C-S	With shear	4.148	4.462	4.508	4.518	4.519	4.519
	No shear	3.868	4.173	4.198	4.206	4.206	4.206
C-C	With shear	2.558	2.648	2.701	2.709	2.708	2.708
	No shear	2.281	2.371	2.393	2.400	2.400	2.400
2. Critical buckling load (*kN*)							
S-S	With shear	400.826	351.215	351.064	351.064	351.064	351.064
C-F	With shear	88.490	87.891	87.891	87.891	87.891	87.891
C-S	With shear	722.958	716.784	716.765	716.765	716.765	716.765
C-C	With shear	1466.429	1397.018	1396.296	1396.294	1396.294	1396.294

Table 3. Maximum deflection of isotropic simply supported I-beams subjected to the concentrated transverse load acting at mid-span (*mm*)

Reference	No shear	With shear
Present	39.8590	39.9465
Kim and Lee [16]	39.8900	40.1700

Table 4. Maximum deflections of cantilever FG I-beams ($h_1 = h_2 = h_3 = h = 0.002m$, $b_1 = 20h$, $b_2 = 10h$, $b_3 = 40h$, $L = 2.5m$, $\alpha_1 = 0.9$, $\alpha_2 = 0.1$, $\alpha_3 = 0.4$, S1-section) subjected to the concentrated transverse load at the free end.

Reference	p								
	0	0.5	1	2	5	10	20	30	50
Present (With shear)	1.2740	1.4439	1.5521	1.6831	1.8461	1.9346	1.9904	2.0112	2.0288
Kim and Lee [16] (With shear)	1.2732	1.4466	1.5566	1.6890	1.8520	1.9395	1.9941	2.0144	2.0315
Present (No shear)	1.2725	1.4422	1.5503	1.6811	1.8440	1.9325	1.9882	2.0090	2.0265
Kim and Lee [16] (No shear)	1.2725	1.4458	1.5558	1.6881	1.8510	1.9341	1.9931	2.0133	2.0304

Table 5. Maximum deflections of cantilever composite I-beams under the concentrated transverse load at the free end (*mm*)

Reference	k_z	$g_z\,(kN)$			
	(kN/m^2)	0	100	200	300
Present (With shear)	0	122.6795	2.2974	1.1792	0.7951
	10	17.2179	1.9626	1.0806	0.7483
	20	10.2502	1.7250	0.9999	0.7076
	30	7.5831	1.5481	0.9324	0.6720
	40	6.1307	1.4107	0.8753	0.6404
Present (No shear)	0	122.5620	2.2890	1.1737	0.7909
	10	17.2146	1.9556	1.0759	0.7445
	20	10.2521	1.7198	0.9957	0.7042
	30	7.5860	1.5437	0.9287	0.6688
	40	6.1337	1.4070	0.8719	0.6375
Kim and Lee [4] (No shear)	0	122.5600	2.2938	1.1771	0.7936
	10	17.2040	1.9600	1.0791	0.7471
	20	10.2370	1.7237	0.9987	0.7067
	30	7.5714	1.5471	0.9315	0.6712
	40	6.1200	1.4100	0.8745	0.6398

Table 6. Mid-span deflections of FG I-beams subject to the concentrated transverse load acting at mid-span ($h_1 = h_2 = h_3 = h = 0.002m$, $b_1 = 20h$, $b_2 = 10h$, $b_3 = 40h$, $\alpha_1 = 0.9, \alpha_2 = 0.1, \alpha_3 = 0.4$, $P_z = 10kN$, S1-section) (mm)

L/b_3	BC	Present	p								
			0	0.5	1	2	5	10	20	30	50
10	S-S	With shear	1.2935	1.4655	1.5749	1.7070	1.8710	1.9599	2.0158	2.0367	2.0543
		No shear	1.2391	1.4043	1.5095	1.6369	1.7955	1.8816	1.9359	1.9561	1.9732
	C-F	With shear	2.5885	2.9328	3.1516	3.4159	3.7441	3.9221	4.0340	4.0757	4.1109
		No shear	2.4791	2.8097	3.0202	3.2750	3.5923	3.7647	3.8733	3.9138	3.9480
	C-S	With shear	0.5965	0.6741	0.7241	0.7843	0.8590	0.8994	0.9248	0.9344	0.9421
		No shear	0.5416	0.6138	0.6598	0.7155	0.7848	0.8224	0.8462	0.8550	0.8625
	C-C	With shear	0.3625	0.4098	0.4405	0.4767	0.5210	0.5458	0.5610	0.5686	0.5702
		No shear	0.3098	0.3503	0.3771	0.4087	0.4478	0.4699	0.4835	0.4905	0.4916
20	S-S	With shear	10.0213	11.3569	12.2070	13.2353	14.5148	15.2096	15.6471	15.8102	15.9480
		No shear	9.9125	11.2344	12.0763	13.0952	14.3638	15.0531	15.4872	15.6492	15.7859
	C-F	With shear	20.0513	22.7236	24.4245	26.4821	29.0420	30.4323	31.3075	31.6340	31.9097
		No shear	19.8325	22.4773	24.1617	26.2003	28.7384	30.1176	30.9861	31.3102	31.5837
	C-S	With shear	4.4396	5.0308	5.4069	5.8615	6.4268	6.7332	6.9264	6.9984	7.0580
		No shear	4.3326	4.9104	5.2783	5.7237	6.2783	6.5795	6.7692	6.8400	6.8986
	C-C	With shear	2.5772	2.9206	3.1394	3.4005	3.7291	3.9059	4.0185	4.0599	4.0948
		No shear	2.4717	2.8018	3.0127	3.2646	3.5826	3.7541	3.8635	3.9037	3.9377

Table 7. Mid-span deflections of FG I-beams subject to the concentrated transverse load acting at mid-span ($h_1 = h_2 = h_3 = h = 0.002m$, $b_1 = 20h$, $b_2 = 10h$, $b_3 = 40h$, $\alpha_1 = \alpha_2 = \alpha_3 = 0.1$, $P_z = 10kN$, S2-section) (mm)

L/b_3	BC	Present	p								
			0	0.5	1	2	5	10	20	30	50
10	S-S	With shear	1.2935	1.6192	1.8524	2.1640	2.6018	2.8653	3.0411	3.1089	3.1670
		No shear	1.2391	1.5511	1.7745	2.0730	2.4924	2.7448	2.9132	2.9781	3.0338
	C-F	With shear	2.5885	3.2403	3.7069	4.3306	5.2066	5.7338	6.0859	6.2214	6.3377
		No shear	2.4791	3.1033	3.5503	4.1476	4.9866	5.4915	5.8287	5.9585	6.0698
	C-S	With shear	0.5965	0.7449	0.8522	0.9957	1.1970	1.3181	1.3992	1.4303	1.4571
		No shear	0.5416	0.6780	0.7756	0.9061	1.0894	1.1996	1.2733	1.3017	1.3261
	C-C	With shear	0.3625	0.4529	0.5178	0.6032	0.7274	0.8015	0.8492	0.8679	0.8868
		No shear	0.3098	0.3867	0.4422	0.5151	0.6212	0.6846	0.7251	0.7411	0.7576
20	S-S	With shear	10.0213	12.5448	14.3516	16.7663	20.1576	22.1993	23.5617	24.0865	24.5366
		No shear	9.9125	12.4086	14.1958	16.5842	19.9388	21.9583	23.3059	23.8250	24.2702
	C-F	With shear	20.0513	25.1004	28.7155	33.5470	40.3327	44.4163	47.1437	48.1938	49.0944
		No shear	19.8325	24.8265	28.4022	33.1809	39.8926	43.9316	46.6293	47.6680	48.5587
	C-S	With shear	4.4396	5.5575	6.3580	7.4277	8.9302	9.8344	10.4382	10.6708	10.8701
		No shear	4.3326	5.4236	6.2048	7.2487	8.7149	9.5973	10.1866	10.4135	10.6081
	C-C	With shear	2.5772	3.2277	3.6923	4.3142	5.1871	5.7026	6.0618	6.1970	6.3112
		No shear	2.4717	3.0956	3.5411	4.1376	4.9749	5.4688	5.8136	5.9433	6.0528

Table 8. Mid-span deflections of FG I-beams subjected to a uniformed transverse load ($h_1 = h_2 = h_3 = h = 0.002m$, $b_1 = 20h$, $b_2 = 10h$, $b_3 = 40h$, $p = 10$ $q_z = 5kN/m, \alpha_1 = 0.9, \alpha_2 = 0.1, \alpha_3 = 0.4$, S1-section) ($mm$)

BC	k_z	g_z (kN)							
	(kN/m^2)	0	10	20	30	40	50	100	200
S-S	0	7.5989	7.262	6.9537	6.6705	6.4093	6.1678	5.1892	3.9375
	5	7.5534	7.2205	6.9156	6.6354	6.3769	6.1377	5.1679	3.9252
	10	7.5085	7.1795	6.878	6.6007	6.3448	6.108	5.1467	3.9129
	20	7.4203	7.0987	6.8038	6.5323	6.2816	6.0494	5.105	3.8887
	50	7.1675	6.867	6.5905	6.3354	6.0993	5.8801	4.9837	3.8177
	100	6.7823	6.5125	6.2633	6.0323	5.8178	5.6179	4.7938	3.705
C-F	0	25.8034	22.5545	20.154	18.3019	16.825	15.6164	11.7916	8.3485
	5	24.6781	21.7091	19.49	17.7627	16.376	15.2349	11.5861	8.2528
	10	23.6494	20.9266	18.8696	17.2555	15.9512	14.8723	11.388	8.1594
	20	21.836	19.5241	17.7438	16.326	15.1666	14.1982	11.0122	7.9791
	50	17.7855	16.2812	15.0701	14.0706	13.2294	12.5097	10.0251	7.4847
	100	13.6479	12.8015	12.086	11.4713	10.9361	10.4645	8.7346	6.7888
C-S	0	3.0777	3.0117	2.9481	2.8874	2.8367	2.7733	2.5245	2.1426
	5	3.0702	3.0042	2.9411	2.8806	2.8227	2.767	2.5194	2.1389
	10	3.0626	2.9969	2.9341	2.8739	2.8162	2.7608	2.5143	2.1352
	20	3.0474	2.9824	2.9202	2.8606	2.8034	2.7485	2.5041	2.1278
	50	3.0029	2.9398	2.8793	2.8213	2.7657	2.7123	2.474	2.106
	100	2.9315	2.8713	2.8136	2.7582	2.7051	2.6539	2.4253	2.0707
C-C	0	1.5701	1.552	1.5343	1.517	1.5002	1.4837	1.4064	1.2741
	5	1.5681	1.5501	1.5325	1.5153	1.4984	1.482	1.4049	1.2728
	10	1.5662	1.5482	1.5306	1.5134	1.4967	1.4802	1.4033	1.2715
	20	1.5624	1.5445	1.527	1.5099	1.4932	1.4768	1.4003	1.269
	50	1.5511	1.5334	1.5162	1.4993	1.4828	1.4667	1.3911	1.2615
	100	1.5326	1.5153	1.4985	1.482	1.4659	1.4501	1.3762	1.2491

Table 9. Mid-span deflections (W) of FG I-beams subjected to a uniformed transverse load ($h_1 = h_2 = h_3 = h = 0.002m$, $b_1 = 20h$, $b_2 = 10h$, $b_3 = 40h$, $p = 10$ $q_z = 5kN/m, \alpha_1 = \alpha_2 = \alpha_3 = 0.1$, S2-section) ($mm$)

BC	k_z	$g_z\,(kN)$							
	(kN/m^2)	0	10	20	30	40	50	100	200
S-S	0	11.0896	10.3866	9.7671	9.2171	8.7256	8.2837	6.6084	4.702
	5	10.9931	10.3018	9.692	9.1502	8.6656	8.2296	6.5739	4.6844
	10	10.8982	10.2184	9.6182	9.0843	8.6064	8.1762	6.5397	4.667
	20	10.7133	10.0556	9.4737	8.9553	8.4905	8.0714	6.4723	4.6325
	50	10.1942	9.5966	9.0651	8.5891	8.1605	7.7725	6.2784	4.5319
	100	9.432	8.918	8.4569	8.0409	7.6639	7.3205	5.9795	4.3735
C-F	0	37.6545	31.186	26.9089	23.8514	21.5439	19.7315	14.3615	9.8633
	5	35.307	29.6087	25.7585	22.965	20.8336	19.1455	14.0705	9.7359
	10	33.2423	28.1878	24.7057	22.1444	20.1703	18.5945	13.7914	9.6118
	20	29.7789	25.7307	22.8462	20.6731	18.9672	17.586	13.2665	9.3734
	50	22.7659	20.4511	18.6788	17.268	16.1126	15.1446	11.9149	8.7263
	100	16.4764	15.3377	14.3998	13.6096	12.9294	12.3398	10.2052	7.8329
C-S	0	4.4949	4.355	4.2237	4.1002	3.9839	3.8742	3.4068	2.7489
	5	4.4785	4.3396	4.2092	4.0866	3.9711	3.8621	3.3975	2.7428
	10	4.4623	4.3244	4.1949	4.0731	3.9584	3.8501	3.3882	2.7367
	20	4.4303	4.2943	4.1666	4.0464	3.9332	3.8262	3.3697	2.7246
	50	4.3368	4.2064	4.0838	3.9683	3.8593	3.7563	3.3154	2.689
	100	4.1894	4.0676	3.9529	3.8446	3.7422	3.6453	3.2286	2.6317
C-C	0	2.2954	2.2569	2.2198	2.1839	2.1491	2.1155	1.9621	1.7144
	5	2.2913	2.253	2.216	2.1802	2.1455	2.112	1.9591	1.7121
	10	2.2872	2.249	2.2121	2.1765	2.1419	2.1085	1.9561	1.7098
	20	2.2791	2.2412	2.2045	2.1691	2.1348	2.1016	1.9501	1.7052
	50	2.2551	2.2179	2.182	2.1473	2.1137	2.0811	1.9324	1.6916
	100	2.2161	2.1802	2.1455	2.1119	2.0794	2.0478	1.9036	1.6694

Table 10. Critical buckling loads (kN) of FG I-beams ($h_1 = h_2 = h_3 = h = 0.005m$, $b_1 = b_2 = 0.1m$, $b_3 = 0.2m$, $L = 2.5m$, $\alpha_1 = \alpha_2 = \alpha_3 = 0.4$, S2-section) with various boundary conditions

p	Present (With shear)				Lanc et al. [11] (No shear)			
	S-S	C-F	C-S	C-C	S-S	C-F	C-S	C-C
0	422.355	105.725	862.488	1680.787	423.296	105.773	867.292	1705.050
0.25	388.279	97.195	792.902	1545.182	389.143	97.239	797.316	1567.480
0.5	365.571	91.510	746.530	1454.814	366.385	91.552	750.687	1475.810
1	337.199	84.408	688.592	1341.907	337.951	84.447	692.428	1361.280
2	308.845	77.311	630.692	1229.074	309.533	77.346	634.203	1246.810
5	280.517	70.219	572.842	1116.339	281.143	70.252	576.034	1132.450
10	267.650	66.999	546.568	1065.136	268.247	67.030	549.611	1080.500
20	260.301	65.159	531.560	1035.890	260.881	65.189	534.520	1050.840
30	257.694	64.506	526.236	1025.514	258.268	64.536	529.165	1040.310
50	255.547	63.969	521.852	1016.971	256.116	63.998	524.757	1031.640

Table 11. Critical buckling loads (*kN*) of FG S-S I-beams ($h_1 = h_2 = h_3 = h = 0.005m$, $b_1 = b_2 = 0.1m$, $b_3 = 0.2m$, $L = 2.5m$, $\alpha_1 = \alpha_2 = 0.7$, $\alpha_3 = 0.4$, S1-section)

p	Present	Reference				
		Kim and Lee [18]		Nguyen et al. [63]		Lanc et al. [11]
	With shear	With shear	No shear	With shear	No shear	No shear
0	422.355	422.359	423.083	421.633	423.079	423.296
0.25	405.212	405.208	405.933	404.154	405.602	406.130
0.5	393.792	393.783	394.515	392.508	393.960	394.692
1	379.529	379.533	380.286	377.958	379.420	380.412
2	365.285	365.280	366.056	363.420	364.899	366.150
5	351.064	351.058	351.825	348.899	350.404	351.914
10	344.610	344.601	345.333	342.305	343.826	345.451
20	340.925	340.906	341.605	338.539	340.070	341.762
30	339.618	339.596	340.278	-	-	340.455
50	338.542	338.522	339.188	-	-	339.377

Table 12. Critical buckling loads (*kN*) of FG C-F I-beams ($h_1 = h_2 = h_3 = h = 0.005m$, $b_1 = b_2 = 0.1m$, $b_3 = 0.2m$, $L = 2.5m$, $\alpha_1 = \alpha_2 = 0.7$, $\alpha_3 = 0.4$, S1-section)

p	Present	Reference				
		Kim and Lee [18]		Nguyen et al. [63]		Lanc et al. [11]
	With shear	With shear	No shear	With Shear	No shear	No shear
0	105.725	105.725	105.771	105.679	105.770	105.773
0.25	101.436	101.435	101.483	101.310	101.401	101.484
0.5	98.579	98.577	98.629	98.399	98.490	98.626
1	95.011	95.013	95.072	94.763	94.855	95.057
2	91.448	91.448	91.514	91.132	91.225	91.494
5	87.891	87.891	87.957	87.507	87.601	87.936
10	86.277	86.277	86.334	85.861	85.957	86.321
20	85.356	85.353	85.403	84.922	85.018	85.400
30	85.029	85.025	85.071	-	-	85.073
50	84.759	84.757	84.799	-	-	84.804

Table 13. Critical buckling loads (*kN*) of FG C-S I-beams ($h_1 = h_2 = h_3 = h = 0.005m$, $b_1 = b_2 = 0.1m$, $b_3 = 0.2m$, $L = 2.5m$, $\alpha_1 = \alpha_2 = 0.7$, $\alpha_3 = 0.4$, S1-section).

p	Present	Reference		
		Kim and Lee [18]		Lanc et al. [11]
	With shear	With shear	No shear	No shear
0	862.488	862.202	865.523	867.292
0.25	827.449	827.152	830.439	832.121
0.5	804.106	803.804	807.080	808.686
1	774.953	774.678	777.970	779.427
2	745.835	745.545	748.857	750.207
5	716.765	716.470	719.741	721.037
10	703.570	703.270	706.458	707.795
20	696.036	695.717	698.830	700.237
30	693.364	693.037	696.115	697.558
50	691.164	690.842	693.884	695.351

Table 14. Critical buckling loads (*kN*) of FG C-C I-beams ($h_1 = h_2 = h_3 = h = 0.005m$, $b_1 = b_2 = 0.1m$, $b_3 = 0.2m$, $L = 2.5m$, $\alpha_1 = \alpha_2 = 0.7$, $\alpha_3 = 0.4$, S1-section).

p	Present	Reference				
		Kim and Lee [18]		Nguyen et al. [63]		Lanc et al. [11]
	With shear	With shear	No shear	With shear	No shear	No shear
0	1680.787	1680.840	1692.352	1669.413	1692.317	1705.050
0.25	1612.391	1612.410	1623.751	1599.491	1622.408	1635.900
0.5	1566.824	1566.830	1578.078	1552.860	1575.838	1589.830
1	1509.909	1509.950	1521.156	1494.551	1517.678	1532.310
2	1453.059	1453.060	1464.229	1436.213	1459.595	1474.860
5	1396.294	1396.270	1407.293	1377.838	1401.613	1417.520
10	1370.527	1370.490	1381.317	1351.288	1375.299	1391.480
20	1355.814	1355.730	1366.399	1336.111	1360.275	1376.630
30	1350.595	1350.500	1361.089	-	-	1371.360
50	1346.982	1346.210	1356.727	-	-	1367.020